Article

Developmental Cell

# Gene copy-number changes and chromosomal instability induced by aneuploidy confer resistance to chemotherapy

## Graphical Abstract

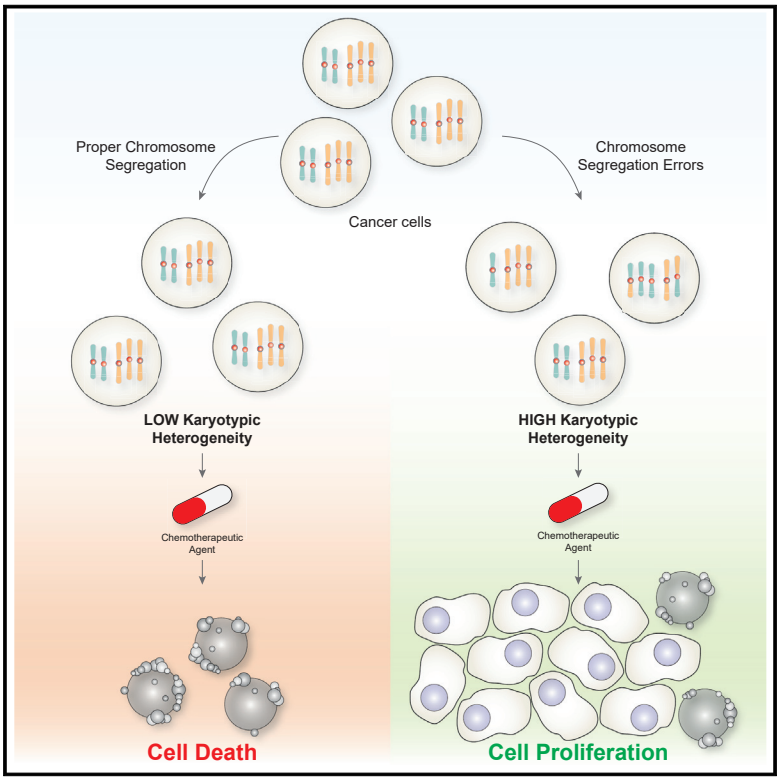


## Highlights

- Genome instability driven by aneuploidy can facilitate chemoresistance
- Chemoresistant cells are characterized by recurrent karyotypes
- Resistance to chemotherapy is dictated by changes in gene copy number
- Chemoresistance is achieved through altered expression of specific proteins

## Authors

Marica Rosaria Ippolito, Valentino Martis, Sara Martin, ..., Uri Ben-David, Floris Foijer, Stefano Santaguida

## Correspondence

stefano.santaguida@ieo.it

## In brief

Ippolito et al. show that induction of chromosome mis-segregation leads to increased karyotypic heterogeneity that could be exploited by cancer cells to survive during chemotherapy. Chemoresistant cells harbor recurrent karyotypes, which impose gene copy-number changes and consequent altered expression of specific proteins crucial for chemoresistance.

Ippolito et al., 2021, Developmental Cell *56*, 1–15
September 13, 2021 
https://doi.org/10.1016/j.devcel.2021.07.006

CellPress

Developmental Cell

CellPress

Article

# Gene copy-number changes and chromosomal instability induced by aneuploidy confer resistance to chemotherapy

Marica Rosaria Ippolito,[1] Valentino Martis,[1,6] Sara Martin,[1,6] Andréa E. Tijhuis,[2] Christy Hong,[2] René Wardenaar,[2] Marie Dumont,[3] Johanna Zerbib,[4] Diana C.J. Spierings,[2] Daniele Fachinetti,[3] Uri Ben-David,[4] Floris Foijer,[2] and Stefano Santaguida[1,5,7,*]

[1]Department of Experimental Oncology at IEO, European Institute of Oncology IRCCS, Via Adamello 16, 20139 Milan, Italy
[2]European Research Institute for the Biology of Ageing, University of Groningen, University Medical Center Groningen, 9713 AV, Groningen, the Netherlands
[3]Institut Curie, PSL Research University, CNRS, UMR144, Paris, France
[4]Department of Human Molecular Genetics and Biochemistry, Faculty of Medicine, Tel Aviv University, Tel Aviv, Israel
[5]Department of Oncology and Hemato-Oncology, University of Milan, Via Santa Sofia 9/1, 20122 Milan, Italy
[6]These authors contributed equally
[7]Lead contact
*Correspondence: stefano.santaguida@ieo.it
https://doi.org/10.1016/j.devcel.2021.07.006

## SUMMARY

Mitotic errors lead to aneuploidy, a condition of karyotype imbalance, frequently found in cancer cells. Alterations in chromosome copy number induce a wide variety of cellular stresses, including genome instability. Here, we show that cancer cells might exploit aneuploidy-induced genome instability and the resulting gene copy-number changes to survive under conditions of selective pressure, such as chemotherapy. Resistance to chemotherapeutic drugs was dictated by the acquisition of recurrent karyotypes, indicating that gene dosage might play a role in driving chemoresistance. Thus, our study establishes a causal link between aneuploidy-driven changes in gene copy number and chemoresistance and might explain why some chemotherapies fail to succeed.

## INTRODUCTION

Chromosome mis-segregation leads to abnormal karyotypes, a condition known as aneuploidy (Santaguida and Amon, 2015). The presence of aneuploid karyotypes affects several processes and has many cellular consequences (Chunduri and Storchová, 2019; Zhu et al., 2018; Weaver and Cleveland, 2008; Levine and Holland, 2018), including genome instability (Ohashi et al., 2015, Passerini et al., 2016, Santaguida et al., 2017, Sheltzer et al., 2011), metabolic alterations (Williams et al., 2008), and proteotoxic stress (Ohashi et al., 2015; Santaguida et al., 2015; Stingele et al., 2012). In humans, aneuploidy is the primary cause of spontaneous abortions and leads to severe developmental defects, such as those present in patients with Down syndrome (trisomy 21) (Roper and Reeves, 2006). Importantly, the aneuploid state is highly prevalent in cancer, and the presence of aneuploid karyotypes correlates with poor patient prognosis (Ben-David and Amon, 2020) and resistance to chemotherapy (Andor et al., 2016; Birkbak et al., 2011; Gómez-Miragaya et al., 2019). Chemotherapy is a central therapeutic strategy for most patients with cancer, and resistance to therapeutic drugs can lead to the failure of this treatment. Thus, studying and understanding chemoresistance is a major challenge in cancer biology. Because of this, there are several ongoing efforts concentrated on understanding the contribution of cell-intrinsic factors—such as genetic alterations and epigenetic changes—as well as cell-extrinsic stimuli—such as cytokines and growth factors—as major players responsible for drug resistance (Vasan et al., 2019). Recent studies have identified an increased resistance of aneuploid cancer cell lines to multiple chemotherapies and to drugs in general (Cohen-Sharir et al., 2021; Replogle et al., 2020). However, very little is known about how and why aneuploidy and the ensuing genomic instability affects the therapeutic outcome. An intriguing hypothesis is that aneuploidy and genome instability provide phenotypic variation, thus increasing heterogeneity within a tumor and driving the ability of cancer cells to adapt to stressful conditions, including chemotherapy. In agreement with this idea, evidence from experiments in yeast has shown that when cells are cultured under strong selective pressure, aneuploid karyotypes can arise as an adaptive mechanism of survival (Rancati et al., 2008; Selmecki et al., 2006). Likewise, in mammalian cells, it has been proposed that aneuploidy is able to provide a proliferative advantage under selective conditions (Rutledge et al., 2016; Salgueiro et al., 2020). Furthermore, copy-number intratumor heterogeneity (ITH) has been associated with worse overall survival in patients (Jamal-Hanjani et al., 2017; Andor et al., 2016). These observations indicate that aneuploidy may be specifically exploited by eukaryotic cells to thrive under unfavorable growth conditions and suggest that karyotypic heterogeneity might negatively affect the ability of patients to benefit from therapeutic drug treatments.

Please cite this article in press as: Ippolito et al., Gene copy-number changes and chromosomal instability induced by aneuploidy confer resistance to chemotherapy, Developmental Cell (2021), https://doi.org/10.1016/j.devcel.2021.07.006



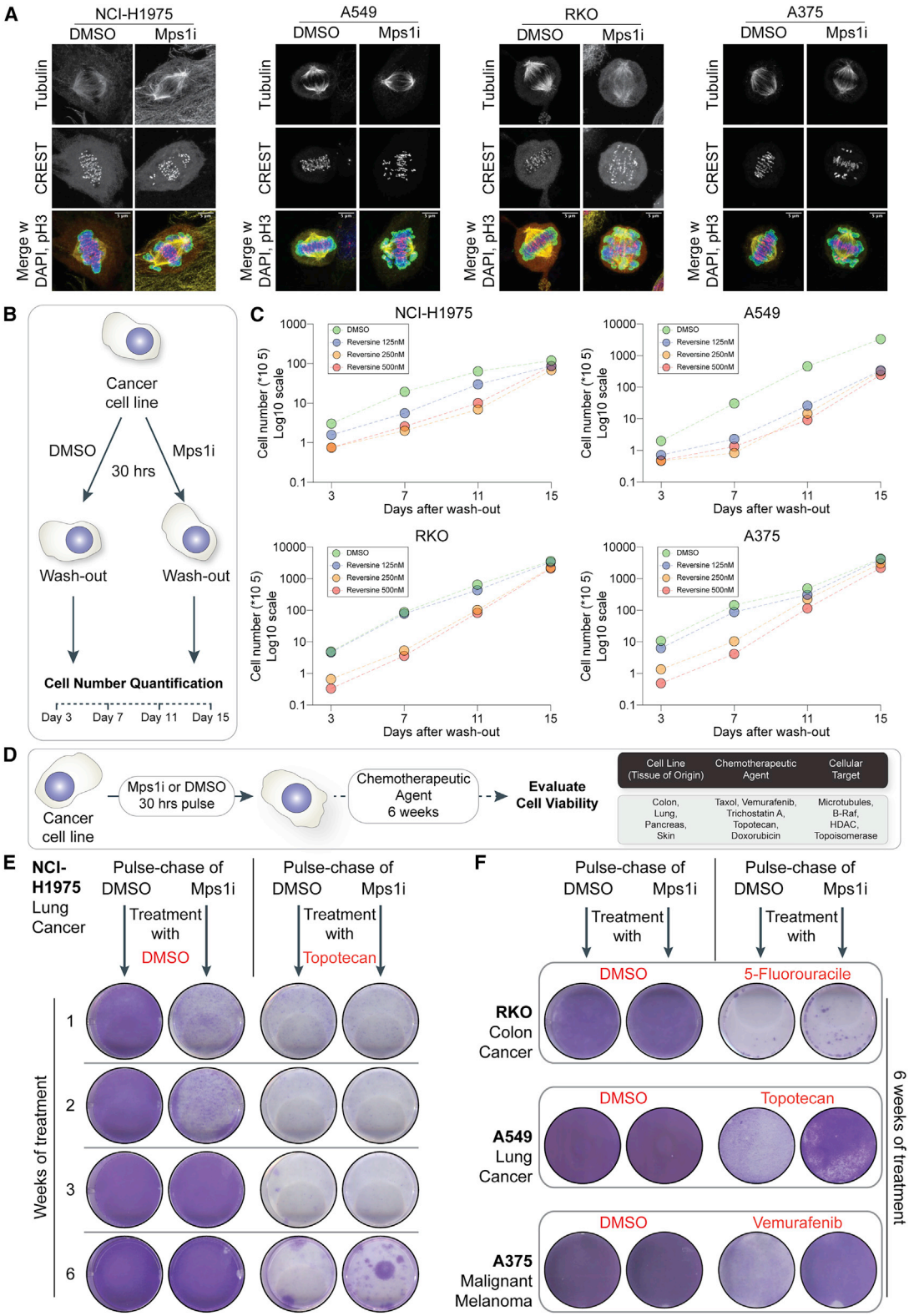


**Figure 1. Elevation of chromosome mis-segregation rate facilitates tolerance to chemoresistance**

(A) Chromosome alignment phenotypes of NCI-H1975, A549, RKO, and A375 cell lines treated with 0.5 μM reversine (Mps1i) or DMSO. Cells were stained with anti-Tubulin, CREST, and Phospho-H3Ser10.

(B) Schematic representation of the experimental setup utilized to evaluate the effect of chromosome mis-segregation induction on the proliferation of a panel of lung, colorectal, and skin cancer cell lines.

*(legend continued on next page)*

To formally test and study the relationship between aneuploidy and chemoresistance, we elevated chromosome mis-segregation rate in a panel of cancer cells prior to exposing them to common clinical chemotherapeutic drugs. We found conditions in which induction of mitotic errors had beneficial effects in the presence of chemotherapeutic agents. Importantly, single-cell-sequencing analysis revealed specific karyotype recurrence in resistant cells. We speculate that aneuploidy-induced genome instability might trigger therapeutic drug resistance through the expansion of karyotype heterogeneity and subsequent convergence onto specific favorable karyotypes that are crucial for cell survival. Clonal karyotypic evolution ensures cell viability through changes in the dosage of specific gene products, such as the therapeutic target, drug efflux pumps, or metabolic enzymes. Therefore, our results provide direct evidence for a role of aneuploidy in driving adaptability during chemotherapy. Finally, given that there are ongoing clinical trials involving agents that elevate chromosome mis-segregation rate (Mason et al., 2017; Pauer et al., 2004; Wang et al., 2019), our study strongly suggests that such a pharmacological approach might not be invariably detrimental for cancer cells but could actually promote cancer cell survival in some cases, highlighting the need to identify the exact conditions in which patients would benefit from such drugs.

## RESULTS

### Elevation of chromosome mis-segregation rate accelerates tolerance to chemoresistance

To begin to investigate whether and how elevation of chromosome segregation errors and the resulting chromosomal instability (CIN) provides a proliferative advantage under conditions of selective pressure, we first induced chromosome mis-segregation in a panel of cancer cell lines by transiently treating them with reversine, a small-molecule inhibitor of the mitotic kinase Mps1 widely used to impair mitotic fidelity (Figures 1A and S1A–S1D; Santaguida et al., 2017, 2010, 2015, 2011). We then removed the drug and monitored cell proliferation over time either in the absence (Figures 1B and 1C) or in the presence of a chemotherapeutic agent and other anti-cancer agents (Figures 1D–1F). In agreement with previous reports (Dobles et al., 2000; Kops et al., 2004; Michel et al., 2004; Santaguida et al., 2017, 2015; Sheltzer et al., 2017; Stingele et al., 2012; Tang et al., 2011; Williams et al., 2008), induction of CIN led to decreased proliferation, observed over a range of concentrations of reversine, corresponding to different degrees of mitotic errors (Figures 1B, 1C, and S1A–S1D). To test the effects of CIN on cell proliferation in the presence of a chemotherapeutic agent, cancer cell lines were exposed to a battery of chemotherapeutic drugs after reversine removal (Figure 1D). We used a panel of cancer cell lines from different tissues of origin, including colon, lung, pancreas, and skin and continuously exposed them for 6 weeks to anti-cancer agents routinely used in the clinic (Figure 1D; Table S1). Among tested conditions, we found combinations in which pretreatment with reversine provided an advantage (in 22% of tested combinations—Table S1), leading to cell survival and colony formation at the end of our experimental protocol. A showcase of this behavior is given by the non-small cell lung cancer (NSCLC) NCI-H1975 treated with the topoisomerase I inhibitor topotecan (Figures 1E and S2A). Under these conditions, induction of CIN through reversine pulse provided permissive conditions for cell survival in presence of topotecan. This was not limited to the particular combination of NCI-H1975 with topotecan but was seen across multiple cell lines and drugs, including the colorectal cancer cell line RKO and the pancreatic cancer cell line PANC1 treated with the thymidylate synthase inhibitor 5-fluorouracil, the lung cancer cell line A549 treated with topotecan, and the malignant melanoma cell line A375 treated with the B-Raf inhibitor vemurafenib (Figures 1F, S2B, and S2C). Interestingly, the amount of CIN induction required for survival upon chemotherapy was dependent on the tested cell line and the chemotherapeutic agent used. A pulse with reversine 500 nM successfully led to the emergence of colonies in NCI-H1975 in the presence of the chemotherapeutic agent, whereas reversine 250 nM pulse was sufficient to achieve similar results in RKO in the presence of the anti-cancer agent (Figures S2D and S2E). This took place despite similar initial responses to Mps1 inhibitor (Mps1i) achieved in the two different cell lines at a given concentration of inhibitor (Figures S1A and S1C), indicating that an optimal degree of chromosomal instability is required to successfully gain chemoresistance. To confirm that these results were not specific to reversine pretreatment, we pulsed NCI-H1975 with AZ3146—a different Mps1 inhibitor (Hewitt et al., 2010)—and obtained similar outcomes (Figure S2F). Importantly, by using a similar experimental setup and chemically unrelated Mps1 inhibitors, Lukow et al. (Lukow et al., 2021 [this issue of *Dev Cell*]) also showed that induction of CIN accelerated the generation of resistant cells able to proliferate in the presence of chemotherapeutic agents. Altogether, our results and those by Lukow and co-workers indicate that despite the fact that induction of CIN is detrimental for cell proliferation, it might be beneficial for cancer cells under conditions of chemotherapy regimen.

### Chemoresistant cells are characterized by the presence of recurrent karyotypes

Interference with the process of chromosome segregation by inhibiting the catalytic function of Mps1 leads to random chromosome gains and losses (Santaguida et al., 2015, 2017; Hoevenaar et al., 2020). Although the resulting chromosome imbalances might have detrimental effects on cell physiology (Figures 1B and 1C), they could also provide phenotypic heterogeneity and might fuel cancer growth, for instance, by sculpting the

(C) Proliferation curves of the indicated cancer cell lines are displayed. Cells were first treated for 30 h with reversine 0.125 μM (blue), 0.250 μM (orange), 0.5 μM (red), or DMSO (green). After drug washout, cells were plated into multi-well plate and counted 3, 7, 11, and 15 days later. Data are shown as average of three biological replicates.

(D) Schematics of experimental setup and list of cancer cell lines utilized to evaluate viability on treatment with a chemotherapeutic, following a pulse of reversine or DMSO. Cell viability was evaluated by crystal violet staining 6 weeks after continuous treatment with the chemotherapeutic agent.

(E and F) Viability assay of NCI-H1975, RKO, A549, and A375 pre-treated for 30 h with DMSO or reversine and then treated for 6 weeks with 0.1 μM Topotecan, 3.5 μM 5-fluoruracile or 1 μM vemurafenib. At the end of the treatment, cells were stained with crystal violet solution. See also Figures S1 and S2.

Please cite this article in press as: Ippolito et al., Gene copy-number changes and chromosomal instability induced by aneuploidy confer resistance to chemotherapy, Developmental Cell (2021), https://doi.org/10.1016/j.devcel.2021.07.006



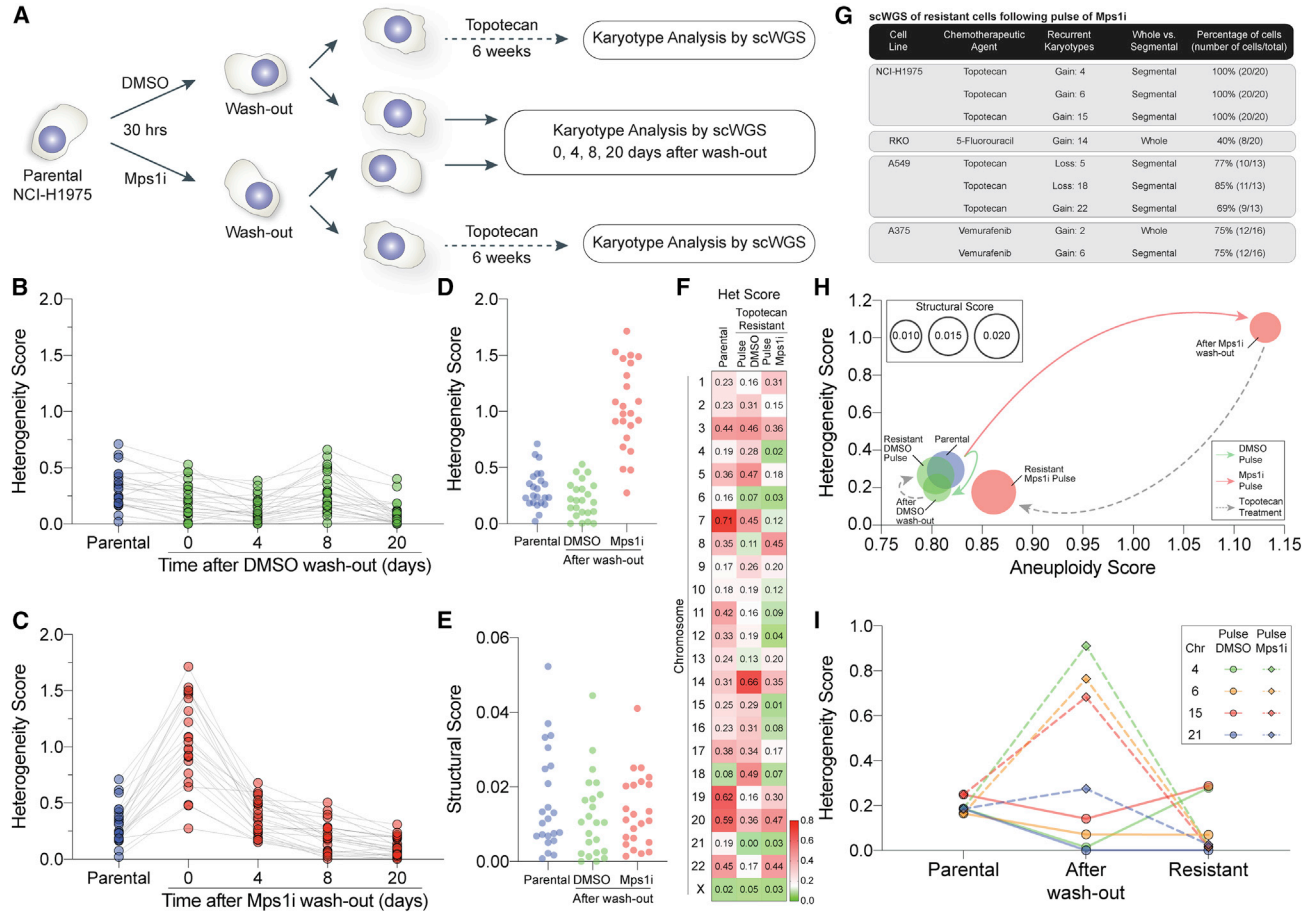


**Figure 2. Chemoresistant cells are characterized by the presence of recurrent karyotypes**

(A) Workflow for the generation of topotecan-resistant NCI-H1975 cells and their sequencing. NCI-H1975 were treated for 30 h with DMSO or reversine. The compound was washed out, and cells were either treated with topotecan for 6 weeks or harvested 0, 4, 8, and 20 days after washout. In both cases, karyotypes analysis was performed by single-cell whole-genome sequencing (scWGS).

(B and C) Heterogeneity scores after DMSO (B) or Mps1i (reversine, C) pulse. Cells were treated as described in (A) and heterogeneity score determined 0, 4, 8, and 20 days after washout. Parental NCI-H1975 are shown as reference. The lanes are connecting the value of heterogeneity scores for a given chromosome across time points.

(D and E) Heterogeneity and structural score of either parental or cells after a pulse of DMSO or Mps1i. Heterogeneity scores are the same as presented in Figures 2B and 2C.

(F) Values of heterogeneity scores for parental NCI-H1975, TRP-DMSO, and TRP-Mps1i are shown. See also Figure S3.

(G) Summary of recurrent karyotypes present in chemoresistance cell lines after a pulse of Mps1i.

(H) Bubble plot showing structural, aneuploidy, and heterogeneity scores for NCI-H1975, either before treatment (light blue), or after washout from either DMSO and subsequent topotecan treatment (light green) or Mps1i and subsequent topotecan treatment (light red). See also Figure S3.

(I) Heterogeneity scores of chromosomes 4, 6, 15, and 21 in parental NCI-H1975 before treatment and right after DMSO or Mps1i washout, and in resistant cells. See also Figure S4.

genome through cumulative haploinsufficiency and triplosensitivity (Davoli et al., 2013). Therefore, we considered that chromosome reshuffling imposed by mitotic errors might expand the karyotypic landscape, thus allowing cancer cells to evolve specific chromosomal assortments that would render them resistant to chemotherapy. To formally test this, we first checked the impact of Mps1i treatment on karyotypic heterogeneity. We decided to focus our attention on NCI-H1975, given the fact that chemoresistance is the main cause for therapeutic failure in NSCLC (Chang, 2011). Karyotype analysis by single-cell whole-genome sequencing (scWGS) (Figure 2A) showed no major changes over time in terms of the heterogeneity score (HS, i.e., the difference in copy number between individual cells in a sample; Bakker et al., 2016) in vehicle-control-treated cells compared with the parental line (Figures 2B and S3A–S3E). At the same time, a transient and massive (~3-fold) increase in the HS for all chromosomes was observed right after Mps1i pulse (time 0 in Figure 2C) compared with parental line (average HS: 0.31 in parental, 1.03 in Mps1i washout at time 0—Figures 2C, 2D, and S3A–S3E), without significant structural rearrangements (Figure 2E, the structural score calculates the number of copy-number changes per megabase for individual cells; also see STAR Methods) in agreement with previous observations (Santaguida et al., 2017; Soto et al., 2017). Next, we examined

the karyotypes of NCI-H1975 cells resistant to topotecan. Analysis of topotecan-resistant cells either DMSO or Mps1i pulsed (named TRP-DMSO—topotecan-resistant pulse DMSO—and TRP-Mps1i—topotecan-resistant-pulse Mpsi1i—respectively) as well as parental line revealed that they were all characterized by both segmental and whole-chromosome aneuploidies (Figures S3A, S3F, and S3G). Remarkably, a feature stood out, whereby the HS of specific chromosomes was lower in resistant cells compared with parental line (Figures 2F, S3A, and S3F). In particular, chromosomes 4, 6, 15, and 21 in TRP-Mps1i were those with the lowest HS (Figure 2F), indicative of the presence of clonal karyotypes (Figure S3F). Interestingly, although the karyotypes of TRP-DMSO and TRP-Mps1i were different (Figure S3F), we also found chromosomes 6 and 21 to have a low HS in TRP-DMSO, suggesting that the ploidy of these chromosomes might be involved in the acquired chemoresistance. Furthermore, to confirm that emergence of chemoresistance associated with clonal karyotypes was not a unique feature of topotecan-treated NCI-H1975, we decided to test whether the Mps1i pulse would favor the emergence of recurrent karyotypes also in other combinations of cell line/chemotherapeutic agent. For this, we used scWGS to determine the karyotypes of RKO cells resistant to 5-FU, A549 to topotecan, and A375 to vemurafenib (Figure 1F) following a DMSO or an Mps1i pulse and compared to their respective parental line (Figures S4A–S4D). As seen in NCI-H1975, scWGS indicated that Mps1i treatment led to massive chromosome segregation errors in all tested cell lines as quantified by an increase in the HS (Figures S4E–S4G; in complete agreement with our analysis of chromosome misalignment and live-cell imaging, Figures S1A–S1C), with no significant changes in structural score (Figures S4E–S4G). Importantly, scWGS analysis showed recurrent aneuploidies in the three cell lines pulsed with Mps1i and exposed to different drugs (Figure 2G). Example of these recurrent aneuploidies in Mps1i-pulsed chemoresistant cells are (1) gain of chromosome 14 in 40% of RKO cells, (2) loss of chromosome 18 in 85% of A549 cells (in the vast majority of the cases in concomitance with loss of chromosome 5 and/or gain of chromosome 22), and (3) gain of chromosomes 6 and 2 in 75% of A375 cells (Figure 2G). Notably, although Mps1i pulse did not induce massive structural rearrangements (Figures S4E–S4G), some of the recurrent karyotypes retrieved in resistant cells involved segmental aneuploidies rather than whole-chromosome gains or losses. We speculate this might be a direct consequence of ongoing replication stress, a feature of aneuploid cells (Ohashi et al., 2015; Passerini et al., 2016; Santaguida et al., 2017). In particular, this state of continuous instability might eventually lead to complex patterns of genome rearrangements and to the generation of segmental aneuploidies, which in turn drives gene copy-number changes (Santaguida et al., 2017; Soto et al., 2017) that could be exploited by cancer cells to survive during chemotherapy. Altogether, our analysis identified recurrent karyotypes in four different cancer cell lines that acquired chemoresistance following Mps1i pulse (Figure 2G). Collectively, these results suggest that in some cases, resistance to chemotherapeutic agents arises from recurrent and clonal aneuploidies generated by induction of transient CIN and these karyotypes might accelerate chemoresistance.

## Increased karyotypic heterogeneity driven by chromosome mis-segregation facilitates chemoresistance

The recurrent patterns of particular chromosomes seen in both NCI-H1975-resistant cell lines could be a consequence of a positive selection—driven by the chemotherapeutic agent—for an underlying karyotype already present in the parental population and/or the result of a process of genome reshaping that drives convergent evolution onto a specific karyotypic state. We reasoned that the former might be a possible scenario for TRP-DMSO cells, whereas the combination of the two conditions might reflect what occurred in TRP-Mps1i. To test this, we analyzed—at the cell-population level—aneuploidy, heterogeneity, and structural scores, which provide the coordinates of the genomic space into which a cell population can navigate (Figure 2H). Notably, Mps1i treatment imposed a departure from the parental genome, allowing the cell population to reach a different karyotypic state, mainly characterized by increased heterogeneity and aneuploidy scores. This state is inherently unstable (Figure 2C), thus providing the possibility to sample different genomic landscapes and empowering rapid genomic drifts during treatment with the chemotherapeutic agent. Indeed, subsequent exposure to topotecan allowed the population to select for one particular state, thereby resulting in lower heterogeneity and aneuploidy scores. On the other hand, as expected, pulsing the parental line with DMSO did not significantly affect these parameters and the resultant resistant cells were as heterogeneous and as aneuploid as the starting population (Figure 2H). These observations, made at the level of the entire genome, are mirrored by the analysis of single chromosomes (Figure 2I). In particular, by tracing the evolution of chromosomes with the lowest HS in resistant cells (chromosomes 4, 6, 15, and 21—Figures 2F and 2I), we noticed that their HS did not undergo major changes when the parental line was pulsed with DMSO, and a similar trend was observed from DMSO washout to the generation of TRP-DMSO (Figure 2I). In striking contrast, HS increased following Mps1i treatment, indicative of karyotypic expansion, and then drastically decreased in TRP-Mps1i, reflecting the convergence on specific karyotypes.

To better delineate the contribution of recurrent chromosomal changes in driving chemoresistance and considering that cancer cell lines are highly heterogeneous to begin with (e.g., Figures S3 and S4), we next tested the impact of aneuploidy induction on chemoresistance of a pseudo-diploid cell line. For this, we exposed untransformed, genomically stable hTERT-immortalized retinal pigment epithelial cells (RPE1-hTERT) to Taxol—a chemotherapeutic agent used in many different types of cancer (Zhu and Chen, 2019)—for 4 weeks after a pulse of Mps1i or vehicle control (Figure 3A). In agreement with previous reports (Santaguida et al., 2017, 2015), Mps1i treatment in RPE1-hTERT cells affected chromosome segregation (Figures S5A and S5B), in turn increasing aneuploidy of daughter cells (Figures 3B and 3C; given the pseudo-diploid nature of RPE1-hTERT, their aneuploidy score—i.e., the faction of the genome deviating from the euploid state within the population [Bakker et al., 2016]—is very low to start with and it dramatically increased on Mps1i treatment). Although RPE1-hTERT pulsed with an Mps1i displayed decreased cell proliferation (Figure S5C; in agreement with Santaguida et al., 2017, 2015), at the same time, they had

Please cite this article in press as: Ippolito et al., Gene copy-number changes and chromosomal instability induced by aneuploidy confer resistance to chemotherapy, Developmental Cell (2021), https://doi.org/10.1016/j.devcel.2021.07.006



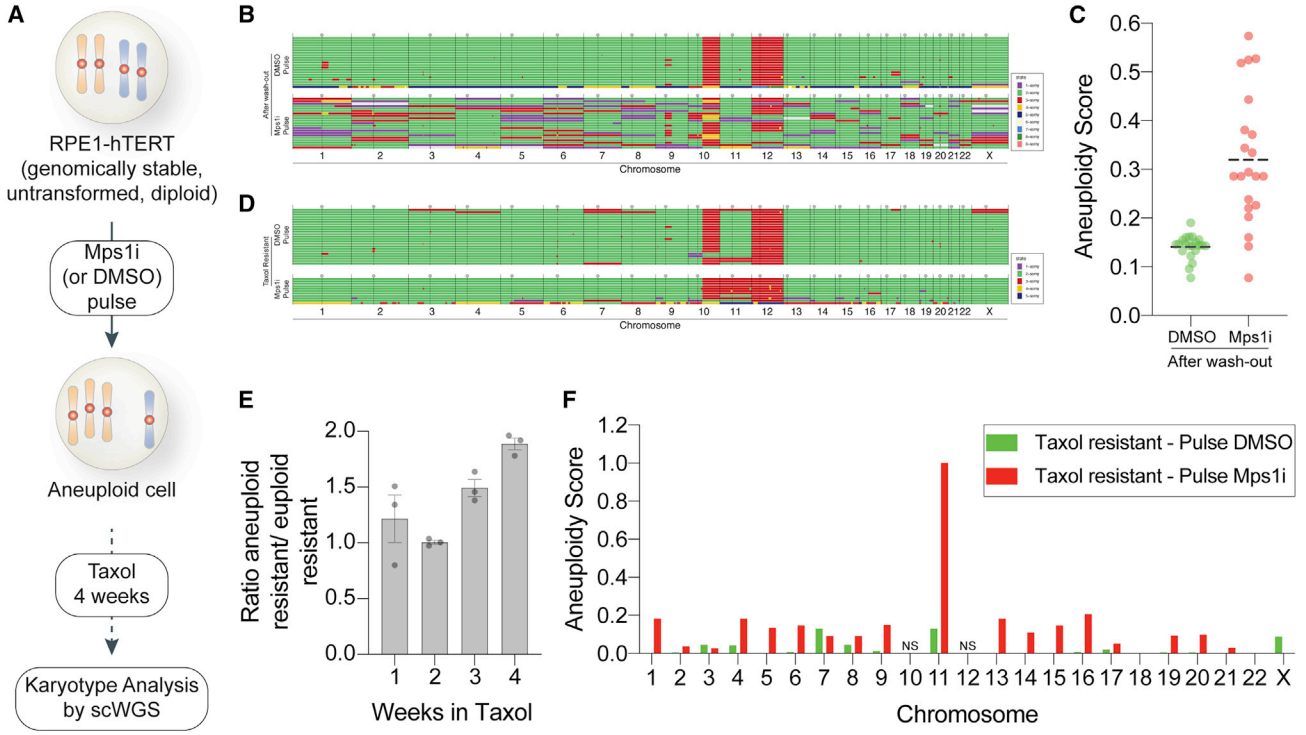


**Figure 3. Aneuploidy induction accelerates chemoresistance in RPE1-hTERT**

(A) Workflow for the generation of Taxol-resistant RPE1-hTERT cells. RPE1 hTERT were treated for 30 h with DMSO or reversine (Mps1i). The compound was washed out and cells were either treated with Taxol for 4 weeks or harvested after washout.

(B) scWGS of RPE1-hTERT 30 h after DMSO or Mps1 pulse. Single cells are represented in rows and chromosomes plotted as columns. Copy-number states are indicated in colors (see legend on the right). RPE1-hTERT cells have clonal gains of 10q and chromosome 12 (Zhang et al., 2015).

(C) Aneuploidy score of RPE1-hTERT cells pulsed with DMSO or Mps1i. The scattered plot shows the average value for each chromosome, and the dashed line marks the mean value of all chromosomes. Chromosomes 10 and 12 are not shown, given the clonal origin of their aneuploidies.

(D) scWGS of Taxol-resistant RPE1-hTERT cells after DMSO or Mps1i pulse. Single cells are represented in rows and chromosomes plotted as columns. Copy-number states are indicated in colors (see legend on the right).

(E) Quantification of viability in Taxol of Mps1i-pulsed (aneuploid) versus DMSO-pulsed (euploid) RPE1-hTERT cells (determined as ratio of crystal violet intensities of Taxol-resistant Mps1i-pulsed cells over Mps1i-pulsed cells versus the ratio of crystal violet intensities of Taxol-resistant DMSO-pulsed cells over DMSO-pulsed cells). Error bars represent mean ± SEM of three biological replicates.

(F) Aneuploidy score of Taxol-resistant DMSO- and Mps1i-pulsed RPE1-hTERT. Chromosomes 10 and 12 are not shown because of clonal origin of these aneuploidies (NS: not shown). See also Figure S5.

a proliferative advantage in presence of the chemotherapeutic agent, compared with vehicle-control-pulsed cells, and displayed recurrent karyotypes (Figures 3D and 3E). In particular, we found a recurrent gain of chromosome 11 in Taxol-resistant cells pulsed with Mps1i, as shown by an increase in the aneuploidy score of this particular chromosome (Figure 3F). Of note, parental cell line displayed a half maximal effective concentration (EC50) of Taxol of 12 nM, whereas the $EC_{50}$ calculated for DMSO- and Mps1i-pulsed-resistant cells had values of 153 and 296 nM, respectively (Figure S5D), indicating a 24-fold increase in chemoresistance in Mps1i-pulsed versus parental cells (Figure S5D). Importantly, trisomy-11-driven chemoresistance was also confirmed in an independent RPE1-hTERT system in which aneuploid derivatives were isolated (Cohen-Sharir et al., 2021). In this system, we generated several aneuploidies by Mps1i treatment and characterized their karyotypes (Cohen-Sharir et al., 2021). One of these aneuploid cell lines harbors a stable gain of chromosome 11 (Figures S5E and S5F), and we found it to be resistant to Taxol compared with its diploid counterpart (Figure S5G—$EC_{50}$ values of 7 and 67 nM in wild-type and trisomy 11 cell line, respectively), further confirming the role of trisomy 11 in resistance to Taxol.

Interestingly, by using a similar experimental setup, Lukow et al. (Lukow et al., 2021 [this issue of *Dev Cell*]) found a loss of chromosome 10 in Taxol-resistant RPE1-hTERT cells, suggesting that chemoresistance to this particular drug might arise from either overexpression of gene(s) located on chromosome 11 or by copy loss of critical genes on chromosome 10. Together, the results obtained in untransformed cells (Figure 3) and those in cancer cells (Figure 1) indicate that recurrent aneuploidies are driver events in chemoresistance and play a pivotal role in fueling resistance to chemotherapeutic agents.

## Aneuploidy-driven gene copy-number changes facilitate evolution of drug resistance

Our data indicate that aneuploidy induction through chemical inhibition of Mps1 kinase activity provides a proliferative advantage under selective pressure of anti-cancer drugs. However,

Please cite this article in press as: Ippolito et al., Gene copy-number changes and chromosomal instability induced by aneuploidy confer resistance to chemotherapy, Developmental Cell (2021), https://doi.org/10.1016/j.devcel.2021.07.006



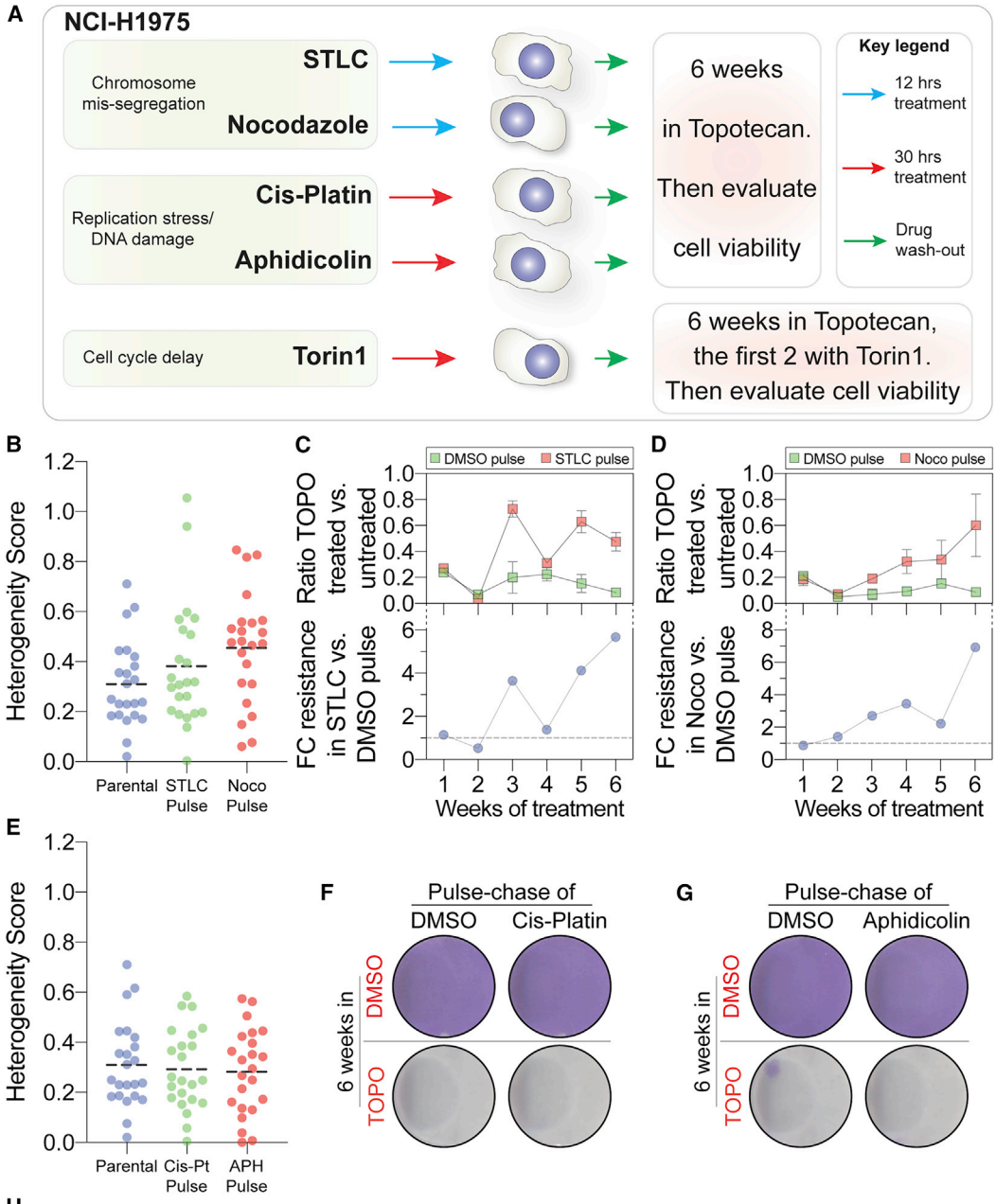


H

| Treatment | Aneuploidy induction | Cell cycle delay | Chemoresistance |
|---|---|---|---|
| Reversine | YES | YES | YES |
| STLC | YES | NO | YES |
| Nocodazole | YES | NO | YES |
| Cis-Platin | NO | NO | NO |
| Aphidicolin | NO | NO | NO |
| Torin1 | NO | YES | NO |

**Figure 4. Aneuploidy-driven gene copy-number changes facilitate evolution of drug resistance**

(A) Schematic representation of the experimental setup utilized to evaluate the effect of chromosome mis-segregation induction, replication stress, and cell-cycle delay on topotecan resistance in NCI-H1975 cell line.

*(legend continued on next page)*

Please cite this article in press as: Ippolito et al., Gene copy-number changes and chromosomal instability induced by aneuploidy confer resistance to chemotherapy, Developmental Cell (2021), https://doi.org/10.1016/j.devcel.2021.07.006



Mps1 kinase activity is strictly required for mitotic checkpoint functioning (Musacchio, 2015), and the ensuing chromosome imbalances acquired upon its inhibition lead to cell-cycle delay in both untransformed and cancer cells (Figures 1C and S5C and Kops et al., 2004). Thus, to disentangle the byproducts of aneuploidy induction mentioned earlier from the effects of karyotypic changes per se, we performed a series of experiments aimed at testing the role of genomic changes in driving chemoresistance.

First, to demonstrate that cellular adaptation in the presence of chemotherapeutic agents was a direct consequence of aneuploidy induction rather than a byproduct of mitotic checkpoint inhibition, we decided to induce chromosome segregation errors independently of checkpoint inactivation. For this, we treated NCI-H1975 cells for 12 h with the mitotic spindle poison S-trityl-L-cysteine (STLC—an inhibitor of the mitotic kinesin Eg5) or the microtubule-depolymerizing drug nocodazole (Figure 4A). These treatments are widely used to achieve checkpoint activation (rather than inhibition, as observed on exposure to Mps1i), leading to mis-segregation of a few chromosomes per cell after spindle poison washout. As a result of this, STLC and nocodazole washout caused an increase in the HS of NCI-H1975 compared with parental line (Figures 4B and S6A) and promoted the acquisition of topotecan resistance after exposure to the drug for 6 weeks (Figures 4C and 4D). These results demonstrate that aneuploidy per se, rather than the method used to generate it, is able to trigger chemoresistance.

Furthermore, we tested whether triggering genome instability by other means not directly related to whole-chromosome mis-segregation would also provide a proliferative advantage. For this, we pulsed NCI-H1975 cells with the alkylating agent cisplatin or the DNA polymerase inhibitor aphidicolin (Figures 4A and S6B–S6D) before exposure to topotecan. We found that these genome-instability-inducing agents did not induce chromosome segregation errors at the concentration used, as judged by lack of significant changes in heterogeneity scores (Figures 4E, S6B, and S6C) and did not facilitate the emergence of colonies following treatment with the chemotherapeutic agent (Figures 4F and 4G), suggesting that karyotypic heterogeneity may be a preferred route to chemoresistance in some cell-line-drug combinations.

Finally, we tested whether cell-cycle delay independent of chromosome segregation errors was able to increase chemotherapeutic resistance. Induction of chromosome segregation errors by Mps1i in both cancer and untransformed cells impaired cell proliferation for about 2 weeks after the initial induction of mitotic errors (e.g., Figures 1C and S5C). Exposure of these aneuploid, cell-cycle-delayed cells to a chemotherapeutic agent led to the emergence of drug-resistant colonies (Figures 1E and 1F). To test the role of cell-cycle delay in chemoresistance, we used an experimental setting recapitulating the delays observed upon induction of aneuploidy. In particular, over the course of 6 weeks, we treated cells with a chemotherapeutic agent (or vehicle control) after imposing a cell-proliferation delay for the first 2 weeks (which resembles what observed upon Mps1i treatment) and then allowed for cell proliferation for the remainder of the experiment (Figure 4A). We achieved this by treating NCI-H1975 with the mTOR kinase inhibitor Torin1, which induced a robust cell-cycle arrest, which was relieved after drug washout (Figure S6E). Although Torin1 treatment closely resembled what was observed on Mps1 inhibition in terms of cell proliferation, this did not confer a proliferative advantage in the presence of topotecan (Figure S6E), indicating that cell-cycle delay per se is not sufficient to dictate chemoresistance in this experimental setting. Furthermore, along this line, aneuploidy induction induced by STLC and nocodazole washout did not impose a major cell-cycle delay (Figure S6F); yet, these cells showed resistance to topotecan.

We conclude that aneuploidy-induced gene copy-number changes confer selective advantages in the presence of chemotherapeutic agents and facilitate the emergence of drug-resistant populations. Importantly, this is independent of the experimental setup used to trigger mitotic errors and is not due to cell-cycle delay (Figures 4G and S6G).

## Cancer cells pulsed with Mps1i are more resistant to chemotherapeutic agents

Next, we focused our attention on the characterization of NCI-H1975 topotecan-resistant cells. The observation that TRP-DMSO and TRP-Mps1i share some (but not all) recurrent chromosomes prompted us to consider the extent to which the Mps1i pulse provided tangible benefits on treatment with the chemotherapeutic agent. For this, we calculated the half maximal-effective concentrations ($EC_{50}$) of Topotecan for both TRP-DMSO and TRP-Mps1i as well as for the parental line (Figure 5A–5D). We measured an $EC_{50}$ of 0.3 μM for the parental line (Figure 5A) and $EC_{50}$ values of 1.5 and 6.2 μM for TRP-DMSO and TRP-Mps1i, respectively (Figures 5B and 5C). The $EC_{50}$ value of TRP-DMSO indicates 5-fold increase over the parental line, whereas the value measured for TRP-Mps1i shows a 20-

(B–D) For chromosome mis-segregation, cells were treated for 12 h with STLC or nocodazole. After mitotic shake-off and drug washout, cells were either analyzed for scWGS (B) or exposed to topotecan for 6 weeks (C and D). In (B), the scattered plot shows the average value of heterogeneity score for each chromosome (values for parental cells are the same as presented in Figures 2B and 2D) and the dashed line marks the mean value of all chromosomes. Cell viability was evaluated by crystal violet staining 6 weeks after continuous treatment with the chemotherapeutic agent (C and D). Top panel shows quantification of viability in 0.1 μM topotecan of STLC- (C) or nocodazole-pulsed (D) cells versus DMSO-pulsed NCI-H1975 cells (determined as ratio of crystal violet intensities of topotecan-resistant STLC- or nocodazole-pulsed cells over STLC- or nocodazole-pulsed cells versus the ratio of crystal violet intensities of topotecan-resistant DMSO-pulsed cells over DMSO-pulsed cells). Bottom panel shows fold change of resistance observed over time in cells pulsed with STLC (C) or nocodazole (D), compared with DMSO, determined as the ratio between the values shown in top panel in STLC (C) or nocodazole (D) pulse over DMSO, at a given time point. Dashed line indicates fold change of 1. Error bars represent mean ± SEM of three biological replicates.

(E–G) For induction of replication stress and DNA damage, cells were treated for 30 h with cisplatin or aphidicolin. After drug washout, cells were either analyzed for scWGS (E) or plated into multi-well plate and exposed to topotecan for 6 weeks (F and G). In (E), the scattered plot shows the average value of heterogeneity score for each chromosome (values for parental cells are the same as presented in Figures 2B, 2D, and 4B), and the dashed line marks the mean value of all chromosomes. Cell viability was evaluated by crystal violet staining 6 weeks after continuous treatment with the chemotherapeutic agent (F and G).

(H) A table summarizing the effects of the indicated treatments in terms of aneuploidy induction, cell-cycle delay, and chemoresistance. See also Figure S6.

Please cite this article in press as: Ippolito et al., Gene copy-number changes and chromosomal instability induced by aneuploidy confer resistance to chemotherapy, Developmental Cell (2021), https://doi.org/10.1016/j.devcel.2021.07.006



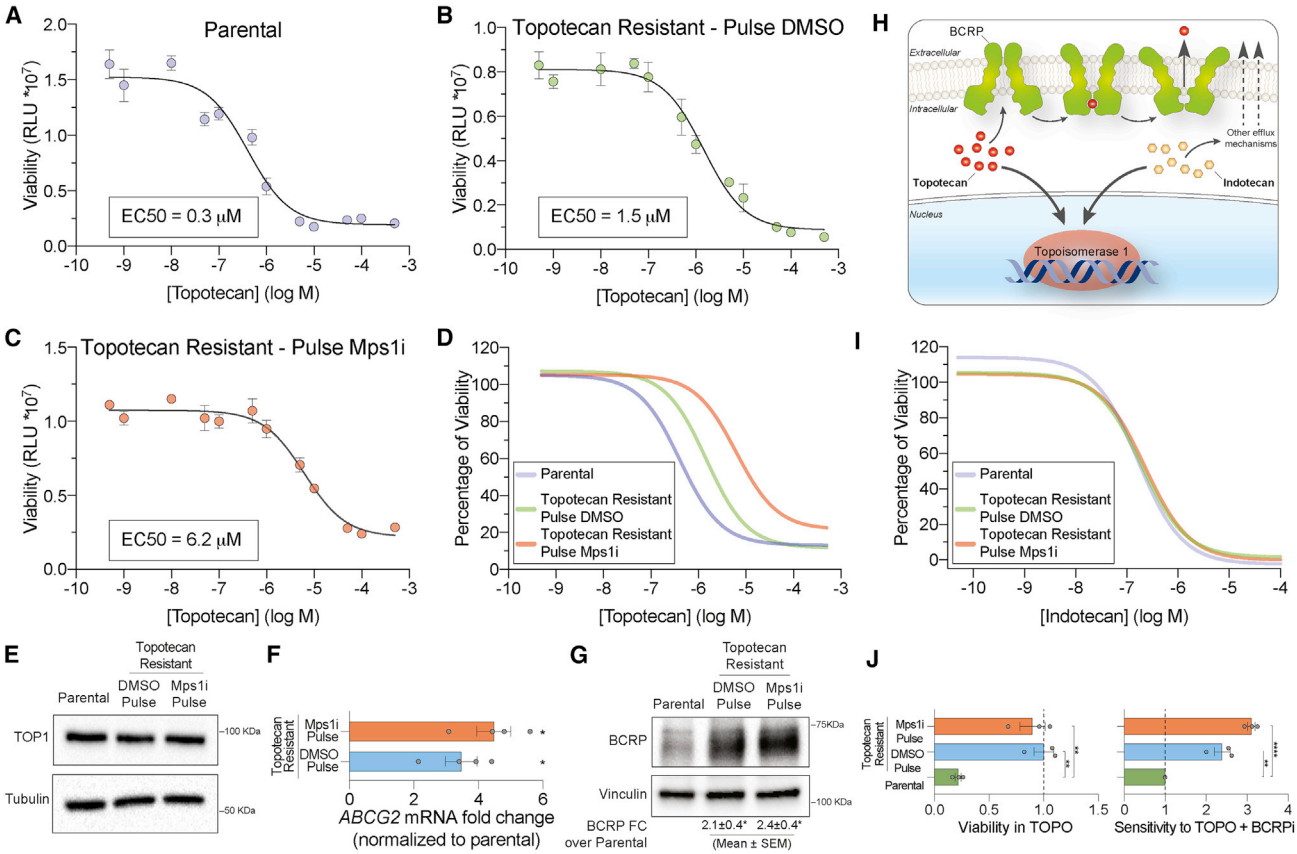


**Figure 5. Cancer cells pulsed with Mps1i are more resistant to chemotherapeutic agents**

(A–D) Viability assays of parental (A), TRP-DMSO (B), and TRP-Mps1i (C) cells treated with the indicated concentrations of topotecan for 72 h and comparison of their profiles (D). The values of calculated half maximal effective concentration ($EC_{50}$) are shown (A–C). RLU stands for relative luminescence unit.

(E) Western blot analysis of topoisomerase 1 protein levels in parental, DMSO, and Mps1i pulse-resistant cells. Tubulin was used as loading control.

(F and G) *ABCG2* mRNA levels (F) and BCRP protein levels (G) were determined in parental NCI-H1975, TRP-DMSO, and TRP-Mps1i cells. In (G), vinculin was used as loading control.

(H) An illustration depicting cellular behavior of topotecan and indotecan. See text for more details.

(I) Viability assay of parental, TRP-DMSO, and TRP-Mps1i cells treated with indotecan.

(J) Quantification of viability in topotecan (determined as ratio of crystal violet intensities of topotecan-treated cells over DMSO-treated cells) and reacquired sensitivity to topotecan in presence of BCRPi (measured as ratio of crystal violet intensities of topotecan-treated cells over topotecan + BCRPi co-treatment). Data show mean ± SEM; *p < 0.05, **p < 0.01, ***p < 0.001, ****p < 0.0001, Wilcoxon rank-sum (F) or Student's t test (G and J). See also Figure S7.

fold increase (Figure 5D). These results indicate that reshaping of the genetic landscape induced by Mps1i treatment provided a substantial change in the ability of cells to survive under selective pressure (Figure 1E).

Next, we investigated the mechanism underlying chemoresistance in TRP-DMSO and TRP-Mps1i. A major determinant of chemoresistance, often seen in cancer cells, is provided by the overexpression of the therapeutic drug target (Holohan et al., 2013). However, when we measured the levels of topoisomerase 1—the target of topotecan—we did not find a difference between parental and resistant cell lines (Figure 5E). We then considered another well-known mechanism of chemoresistance, which is overexpression of drug efflux pumps (Holohan et al., 2013). These are transmembrane proteins that include MDR1, MRP1, and BCRP, encoded by *ABC*B1, *ABCC1*, and *ABCG2*, respectively. Efflux pumps have different substrate specificity but share the same mechanism of action, namely an ATP-dependent conformational change mediating the binding to a specific substrate and subsequent extrusion from the cell (Robey et al., 2018). Interestingly, although there was no increase in *ABCB1* and *ABCC1* expression between parental and resistant cell lines (Figure S7A; note we were unable to detect any signal for *ABCB1* transcripts in the tested samples), *ABCG2* mRNA levels were increased in both resistant cell lines (Figure 5F), which in turn led to increased protein expression as well (Figure 5G; similar results were obtained in topotecan-resistant cells obtained through pulse with STLC or nocodazole—Figure S7B).

To define the role of BCRP upregulation in topotecan resistance and to formally rule out the involvement of topoisomerase 1 in the process (e.g., as a result of mutagenic events), we designed and performed a series of experiments. First, because topotecan efflux is mediated by BCRP (Nagashima et al., 2006), we reasoned that a different topoisomerase 1 inhibitor that is not substrate of BCRP provided a simple way to confirm the role of BCRP in topotecan resistance and, at the same

Please cite this article in press as: Ippolito et al., Gene copy-number changes and chromosomal instability induced by aneuploidy confer resistance to chemotherapy, Developmental Cell (2021), https://doi.org/10.1016/j.devcel.2021.07.006



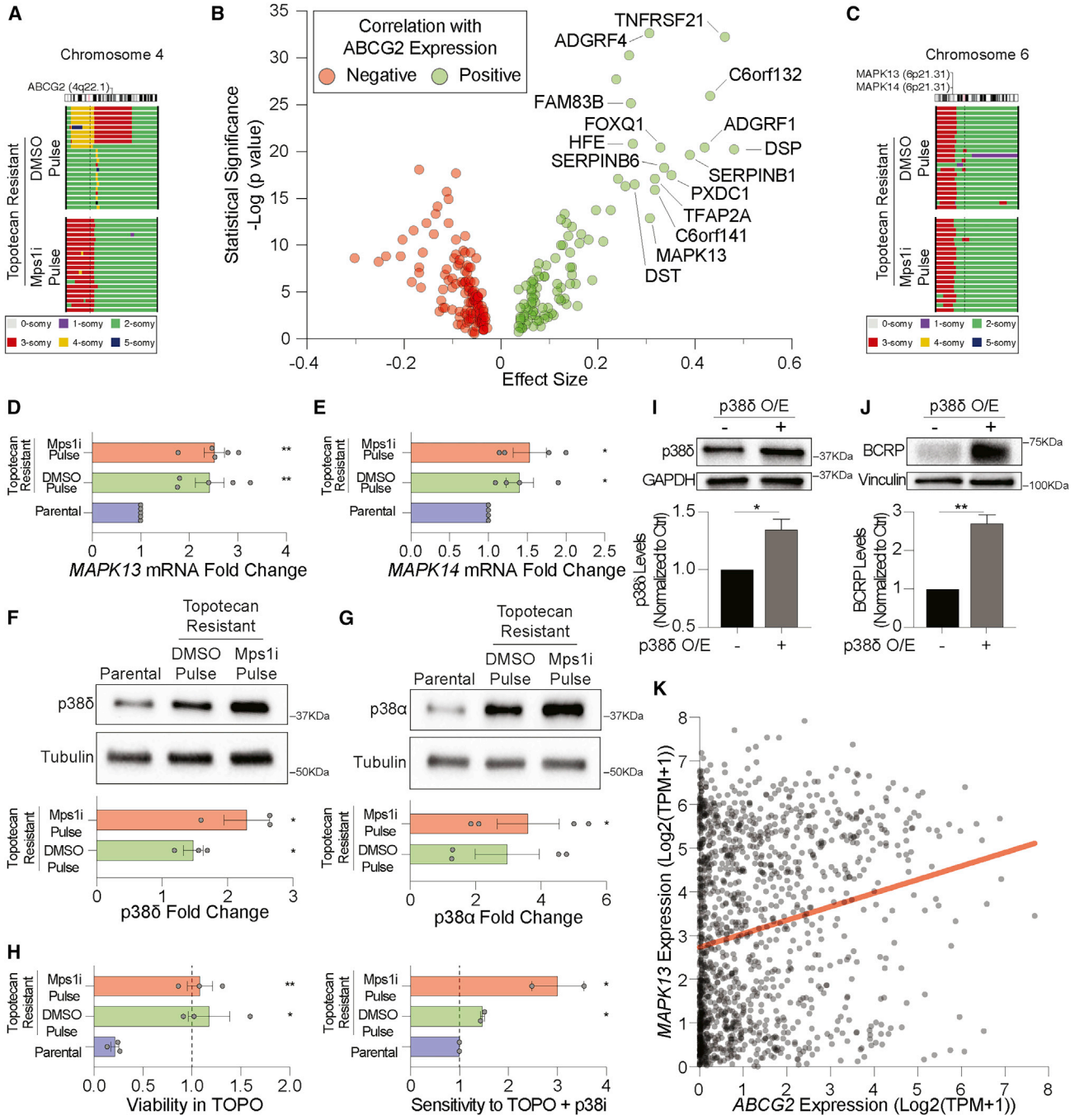


**Figure 6. Aneuploidy-induced upregulation of specific proteins drive chemoresistance**

(A) Chromosomal location of *ABCG2* (4q22.1) in relation to copy state number of TRP-DMSO and TRP-Mps1i. Copy state numbers are indicated in colors (see legend on the bottom).

(B and C) (B) A volcano plot showing the co-expression of genes that reside on chromosome 6 with the expression of *ABC*G2 chromosomal location of *MAPK13* and *MAPK14* (6p21.31) in relation to copy-state number of TRP-DMSO and TRP-Mps1i. Copy-number states are indicated in colors (see legend on the bottom). Chromosome 4 (A) and 6 (C) are the same sequencing results displayed in Figure S3F.

(D and E) *MAPK13* (D) and *MAPK14* (E) mRNA levels were determined in parental NCI-H1975, TRP-DMSO, and TRP-Mps1i cells. Error bars represent mean ± SEM of at least four biological replicates.

(F and G) p38delta (F) and p38alpha (G) protein levels were determined in parental NCI-H1975, TRP-DMSO, and TRP-Mps1i cells. Tubulin was used as loading control. Western blot quantification is shown on the bottom.

(H) Quantification of viability in topotecan (determined as ratio of crystal violet intensities of topotecan-treated cells over DMSO-treated cells) and reacquired sensitivity to topotecan in presence of p38i (measured as ratio of crystal violet intensities of topotecan-treated cells over topotecan + p38i co-treatment).

*(legend continued on next page)*

Please cite this article in press as: Ippolito et al., Gene copy-number changes and chromosomal instability induced by aneuploidy confer resistance to chemotherapy, Developmental Cell (2021), https://doi.org/10.1016/j.devcel.2021.07.006





time, to exclude the involvement of topoisomerase 1. If topotecan-resistant cells were also resistant to such a drug, it would suggest that BCRP upregulation was a passenger event. In contrast, if they were sensitive to such a drug as much as parental cells, it would favor a model in which BCRP upregulation has a key role in chemoresistance. The feasibility of this idea was investigated by using indotecan (Pommier and Cushman, 2009), a topoisomerase 1 inhibitor chemically unrelated to topotecan and not transported by BCRP (Figure 5H). Quite revealingly, $EC_{50}$ values of indotecan were very similar in topotecan-resistant cells and parental line (Figure 5I). This suggests that topoisomerase 1 was still functional in resistant cells and can be efficiently inhibited and indicates that BCRP upregulation was not sufficient to mediate indotecan resistance but crucial in topotecan resistance. Furthermore, in agreement with the central role of BCRP in drug resistance, its chemical inhibition restored sensitivity to topotecan in resistant cell lines (Figures 5J and S7C). Finally, chemoresistance could be often achieved through genetic mutations of crucial cellular players able to decrease drug efficacy at different levels (e.g., drug target, metabolic enzymes, efflux mechanisms). Thus, to exclude the presence of driving mutations in resistant cells, we performed whole-exome sequencing (WES) of parental, TRP-DMSO, and TRP-Mps1i cells. Among retrieved mutations, we did not find any in relevant genes linked to chemoresistance (including *TOP1* and *ABCG2*—Table S2) suggesting that genetic mutations were not involved in drug resistance in this case.

In conclusion, our data strongly indicate that resistance to topotecan in TRP-Mps1i and TRP-DMSO was mediated by BCRP upregulation, with no changes in other potential players, including the drug target.

### Aneuploidy-induced upregulation of specific proteins drives chemoresistance

Our results demonstrate that BCRP upregulation drives topotecan resistance in TRP-Mps1i and TRP-DMSO (Figure 5J). Intriguingly, the chromosomal region encompassing *ABCG2*—*q* arm of chromosome 4—was not amplified at all in TRP-Mps1i and was amplified in only in a fraction of TRP-DMSO cells (Figure 6A). A potential reason for this lack of amplification might be provided by the identity of genes present on this arm of chromosome 4, which have known tumor-suppressor functions (e.g., TET2 [4q24], FAT4 [4q28.1], FBXW7 [4q31.3], and FAT1 [4q35.2]). This led us to speculate that because of these genes, resistant cells might have found other ways to upregulate a particular gene of interest, such as *ABC*G2, without amplifying the corresponding chromosomal region, thus avoiding the load of extra copies of tumor suppressors. To identify potential proteins/pathways responsible for *ABCG2* upregulation, we searched for genes whose expression positively correlates with *ABCG2* expression (Figure 6B), by interrogating the Cancer Cell Line Encyclopedia (CCLE) gene expression dataset (Ghandi et al., 2019). This led to the creation of a list of genes that positively or negatively correlated with *ABCG2* expression in a panel of 1,365 cancer cell lines (Table S3). To narrow down our search, we decided to focus on genes located on gained chromosomal regions with a high recurrence (i.e., low HS) in resistant cells. Chromosome 6 for which the vast majority of *p* arm was gained as product of a translocation with chromosome 11 in almost all resistant cells (Figures S7D–S7G) met these requirements. Therefore, we concentrated on the top 15 genes co-expressing with *ABCG2* and residing on chromosome 6 (Figure 6B). Among them, *MAPK13* stood out, mainly for two reasons. First, *MAPK13*, together with its homolog *MAPK14*, is located within the minimal-gained region of chromosome 6p in both resistant cell lines. Second, *MAPK13* and *MAPK14* encode for the subunits p38delta and p38alpha, respectively, of the stress kinase p38, a member of the MAPK pathway, which has been involved in the regulation of *ABCG2* (Xie et al., 2014) and other plasma membrane proteins (Schonhoff et al., 2016). In agreement with gene copy-number changes dictated by chromosome 6p gain, we found an increase in *MAPK13* and *MAPK14 mRNA* (Figures 6D, 6E, and S7H) as well as in p38alpha and p38delta protein levels in resistant cell lines (Figures 6F and 6G). Importantly, inhibition of p38 kinase activity with two chemically unrelated chemical inhibitors was able to restore sensitivity to topotecan in resistant cells (Figures 6H, S7I, and S7J), pointing at p38 as the main driver of chemoresistance in TRP-DMSO and TRP-Mps1i cells. Notably, this dependency on p38 for sustained chemoresistance was directly linked to BCRP, as p38 inhibition decreased the amount of BCRP localized at the plasma membrane (Figures S7K and S7L).

To determine whether there was a causal link between *MAPK13* copy-number increase and BCRP upregulation, we overexpressed p38delta in NCI-H1975 cells and measured the levels of BCRP. We found that ectopic p38delta overexpression led to a robust increase in the levels of BCRP (Figures 6I and 6J), providing a direct connection between the two. Finally, we interrogated the association between *MAPK13* and *ABCG2* across the CCLE and found a significant correlation between the mRNA expression of the two genes (Figure 6K). Future studies are required to elucidate the nature of the interaction between p38 and BCRP at the molecular level, with potentially important implications for the combinatorial clinical use of p38 and BCRP inhibitors.

Altogether, our data favor a model in which chemoresistance could be achieved through copy-number-neutral increased expression of a crucial player, such as a drug efflux pump, due to the overexpression of a copy-number-gained gene, providing an extra layer of complexity to be considered in clinical efforts to overcome chemoresistance.

## DISCUSSION

Previous work showed that aneuploidy and the ensuing CIN is highly detrimental in all organisms and experimental systems analyzed to date (Kops et al., 2004; Santaguida et al., 2017,

(I and J) p38δ (I) and BCRP (J) protein levels following p38δ overexpression in the NCI-H1975 cell line. GAPDH and vinculin were used as a loading control. Images are representative of three biological replicates. Bottom: quantification of p38δ and BCRP normalized over loading control and presented as fold change over cells without ectopic overexpression.

(K) The correlations between the mRNA expression levels of MAPK13 and ABCG2 in a panel of cancer cell lines. Spearman's $\rho = 0.212$ and $p = 1e{-}14$. *$p < 0.05$, **$p < 0.01$, ***$p < 0.001$, ****$p < 0.0001$, Wilcoxon rank-sum (D and E) or Student's t test (F, G, H, I, and J). See also Figure S7.

Please cite this article in press as: Ippolito et al., Gene copy-number changes and chromosomal instability induced by aneuploidy confer resistance to chemotherapy, Developmental Cell (2021), https://doi.org/10.1016/j.devcel.2021.07.006



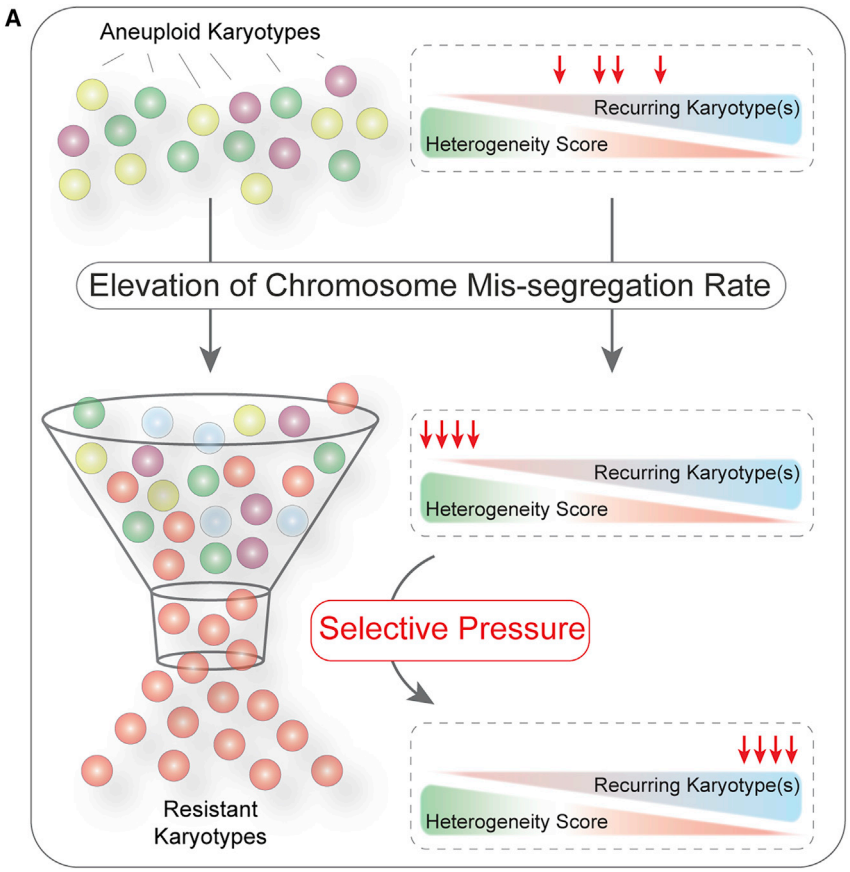


**Figure 7. A model for how aneuploidy-induced genome instability creates permissive conditions under selective pressure**
See text for more details.

2015; Sheltzer et al., 2017; Stingele et al., 2012; Tang et al., 2011; Torres et al., 2007; Williams et al., 2008). On the other hand, recent studies have also suggested that aneuploidy might facilitate cell proliferation under specific conditions. Examples of this include aneuploidy-specific drug resistance in *Candida albicans* (Selmecki et al., 2006, 2009) and *Saccharomyces cerevisae* (Chen et al., 2012, 2015), and trisomy-driven proliferation under stress conditions in colorectal cancer cell lines (Rutledge et al., 2016). These aneuploidy-specific phenotypes might be the consequence of transcriptomic and proteomic changes imposed by specific chromosome gains and losses (Gemoll et al., 2013; Habermann et al., 2007; Pavelka et al., 2010; Santaguida et al., 2017, 2015; Stingele et al., 2012; Torres et al., 2007).

By systematically testing a series of cancer lines exposed to several chemotherapeutic agents, in this study, we have explored the idea that aneuploidy-induced CIN might facilitate the acquisition of resistance to chemotherapy (Table S1). For five combinations of chemotherapeutic agents and cell lines, we have determined the karyotypes of resistant cell lines by scWGS. We show that CIN and the resulting aneuploidy could be exploited by cells to survive under selective pressure, which might explain why aneuploid karyotypes and CIN are a widespread feature of advanced tumors.

Our data suggest a model in which elevation of chromosome mis-segregation rate in a cell population increases karyotypic heterogeneity (Figure 7A). At this stage, the cell population is highly genomically unstable, a condition that might be unfavorable for cell proliferation (e.g., Figures 1C and S5C; in agreement with Kops et al., 2004), but that can provide the ability to widely sample the genomic space and, in the presence of chemotherapeutic agents, eventually find the right karyotypic assortment for chemoresistance (Figure 7A). This might happen through amplification of a chromosomal region encompassing a gene directly involved in chemoresistance, such as the therapeutic drug target or, as in the case presented here with the NCI-H1975 cell line, by overexpressing a gene that upregulates a drug efflux pump. We note that we also found the lung cancer cell line A549 to become resistant to topotecan after a pulse of Mps1i (Figures 1F and S4B). However, topotecan-resistant A549 showed a completely different pattern of recurrent aneuploidies (Figure 2G) compared with NCI-H1975, suggesting that the same chemotherapeutic agent could benefit from different karyotypic assortments, which might depend on the genetic makeup of cancer cells.

Resistance to anti-cancer drugs might be the product of genetic mutations (Vasan et al., 2019). Because our WES analysis did not identify mutations in genes known to be involved in chemoresistance, we concluded that the observed mutations were passenger events. However, it is still possible that mutation(s) we found might play a role in chemoresistance—alone or in combination with recurrent aneuploidies—and future studies will be aimed at clarifying this potential connection.

Several studies showed that cells harboring aneuploidies are slower in cell-cycle progression with a major G1 delay (Kops et al., 2004; Santaguida et al., 2017, 2015; Sheltzer et al., 2017; Stingele et al., 2012; Tang et al., 2011; Torres et al., 2007; Williams et al., 2008). Interestingly, it has been recently proposed that this detrimental effect of aneuploidy on cell proliferation could increase resistance to particular chemotherapeutics (Replogle et al., 2020). This might be a direct consequence of prolonged G1 phase, which would jeopardize the activity of anti-proliferative drugs targeting S or M phase (Replogle et al., 2020). This prompted us to test whether aneuploidy-induced cell-cycle delay was involved in the chemoresistance observed in our study (Figure 4A). Our experiments using the mTOR kinase inhibitor Torin1 to slow down cell cycle indicated that lengthening of G1 was not enough to permit cell proliferation in the presence of chemotherapeutic agent, at least in the combination tested here (Figure S6E). Furthermore, chemoresistance was still observed in aneuploid cells generated by nocodazole and STLC washout, although these treatments did not induce cell-cycle

delay (Figures 4G and S6F). However, we note that it is possible that resistance to certain chemotherapies might be the result of both aneuploidy-induced consequences, namely karyotypic aberrations and cell-cycle delay, which might cooperate with each other to reduce the efficacy of anti-cancer drugs.

Interestingly, our current results in cell lines mimic our previous results in patient-derived xenografts (PDXs), where we found elevated levels of CIN to be associated with chemoresistance (Ben-David et al., 2017). PDXs, however, do not lend themselves easily to functional manipulations. Using cell lines, we were now able to follow the karyotypic evolution of cancer cells exposed to chemotherapeutic agents and demonstrate that the proliferation advantage induced by CIN under conditions of selective pressure is mediated by the selection of an optimal karyotype. For topotecan resistance in NCI-H1975 cells, we provide a molecular link between the selected karyotype and the acquired chemoresistance.

We conclude that aneuploidy and CIN are strong promoters of phenotypic variation. Current therapeutic approaches focus on drugs that increase CIN (Mason et al., 2017; Pauer et al., 2004; Wang et al., 2019). Although these approaches can be valuable, as also demonstrated by increased sensitivity to Taxol in cells undergoing mild chromosome mis-segregation (Janssen et al., 2009), our results demonstrate that developing approaches to decrease CIN (e.g., Orr et al., 2016) are equally important. More research is required to determine which patients may benefit from each of these opposite strategies, which will be instrumental for overcoming chemoresistance.

### Limitations of the study

Although we provide evidence for a direct contribution of recurrent aneuploidies in driving chemoresistance, our work strongly relies on established cancer cell lines. Future studies utilizing chemoresistant primary tumor cells are required to further define the link between aneuploidy-induced gene copy-number changes and chemoresistance.

## STAR★METHODS

Detailed methods are provided in the online version of this paper and include the following:

- KEY RESOURCES TABLE
- RESOURCE AVAILABILITY
  - Lead contact
  - Materials availability
  - Data and code availability
- EXPERIMENTAL MODEL AND SUBJECT DETAILS
  - Cell culture condition and reagents
  - Drug treatments
- METHOD DETAILS
  - Cell proliferation Assay
  - RNA extraction, RT–PCR and qPCR
  - Protein detection by Western blots
  - Retrovirus production and infection of target cells
  - Cell imaging methods
  - Video microscopy
  - Crystal violet assay
  - EC50 assay
  - Plasma membrane purification
  - Multicolor fluorescence in situ hybridization (mFISH)
  - Sample processing for single-cell sequencing
  - Data analysis single-cell sequencing
  - Detection of SNPs and small indels
  - Co-expression analysis of *ABCG2* with genes residing on chromosome 6
- QUANTIFICATION AND STATISTICAL ANALYSIS

## SUPPLEMENTAL INFORMATION

Supplemental information can be found online at https://doi.org/10.1016/j.devcel.2021.07.006.

## ACKNOWLEDGMENTS

We are grateful to Devon Lukow and Jason Sheltzer (CSHL) for sharing data prior to publication. We acknowledge help from Anna Obenauf and Christian Umkehrer (IMP) and Giuseppina De Feudis (IEO). We thank Stephen Taylor (University of Manchester), Mike Hemann (MIT), and members of the Santaguida lab for constructive discussions throughout the project. Work in the Santaguida lab is supported by grants from the Italian Association for Cancer Research (MFAG 2018 - ID. 21665 project), Ricerca Finalizzata (GR-2018-12367077), Fondazione Cariplo, the Rita-Levi Montalcini program from MIUR, and the Italian Ministry of Health with Ricerca Corrente and 5×1000 funds. This work was also supported by a Dutch Cancer Society grant (2017-RUG-11457) to the Foijer lab. Work in the Ben-David lab is supported by grants from the Azrieli Foundation (Faculty Fellow), the Israel Cancer Association (grant #20200111), the Israel Cancer Research Fund (Gesher Award), the Dod CDMRP Career Development Award (grant #CA191148), and the United States – Israel Binational Science Foundation (grant #2019228). D.F. receives salary support from the CNRS and I. Curie. M.D.'s salary is covered by Emergence Grant 2018 from the City of Paris and an HFSP grant.

## AUTHOR CONTRIBUTIONS

Conceptualization, M.R.I. and S.S.; investigation, M.R.I., V.M., S.M., A.E.T., C.H., R.W., M.D., J.Z., and D.C.J.S.; writing, S.S. with input from all authors; funding acquisition and supervision, D.F., F.F., U.B.-D., and S.S. All authors discussed the results and commented on the manuscript.

## DECLARATION OF INTERESTS

The authors declare no competing interests.

Received: November 8, 2020
Revised: May 9, 2021
Accepted: July 9, 2021
Published: August 4, 2021

## REFERENCES

Andor, N., Graham, T.A., Jansen, M., Xia, L.C., Aktipis, C.A., Petritsch, C., Ji, H.P., and Maley, C.C. (2016). Pan-cancer analysis of the extent and consequences of intratumor heterogeneity. Nat. Med. *22*, 105–113.

Bakker, B., Taudt, A., Belderbos, M.E., Porubsky, D., Spierings, D.C., De Jong, T.V., Halsema, N., Kazemier, H.G., Hoekstra-Wakker, K., Bradley, A., et al. (2016). Single-cell sequencing reveals karyotype heterogeneity in murine and human malignancies. Genome Biol. *17*, 115.

Ben-David, U., and Amon, A. (2020). Context is everything: aneuploidy in cancer. Nat. Rev. Genet. *21*, 44–62.

Ben-David, U., Ha, G., Tseng, Y.Y., Greenwald, N.F., Oh, C., Shih, J., Mcfarland, J.M., Wong, B., Boehm, J.S., Beroukhim, R., and Golub, T.R. (2017). Patient-derived xenografts undergo mouse-specific tumor evolution. Nat. Genet. *49*, 1567–1575.

Birkbak, N.J., Eklund, A.C., Li, Q., Mcclelland, S.E., Endesfelder, D., Tan, P., Tan, I.B., Richardson, A.L., Szallasi, Z., and Swanton, C. (2011). Paradoxical relationship between chromosomal instability and survival outcome in cancer. Cancer Res. *71*, 3447–3452.

Chang, A. (2011). Chemotherapy, chemoresistance and the changing treatment landscape for NSCLC. Lung Cancer *71*, 3–10.

Chen, G., Bradford, W.D., Seidel, C.W., and Li, R. (2012). Hsp90 stress potentiates rapid cellular adaptation through induction of aneuploidy. Nature *482*, 246–250.

Chen, G., Mulla, W.A., Kucharavy, A., Tsai, H.J., Rubinstein, B., Conkright, J., Mccroskey, S., Bradford, W.D., Weems, L., Haug, J.S., et al. (2015). Targeting the adaptability of heterogeneous aneuploids. Cell *160*, 771–784.

Chunduri, N.K., and Storchová, Z. (2019). The diverse consequences of aneuploidy. Nat. Cell Biol. *21*, 54–62.

Cingolani, P., Platts, A., Wang, le L., Coon, M., Nguyen, T., Wang, L., Land, S.J., Lu, X., and Ruden, D.M. (2012). A program for annotating and predicting the effects of single nucleotide polymorphisms, SnpEff: SNPs in the genome of Drosophila melanogaster strain w1118; iso-2; iso-3. Fly (Austin) *6*, 80–92.

Cohen-Sharir, Y., Mcfarland, J.M., Abdusamad, M., Marquis, C., Bernhard, S.V., Kazachkova, M., Tang, H., Ippolito, M.R., Laue, K., Zerbib, J., et al. (2021). Aneuploidy renders cancer cells vulnerable to mitotic checkpoint inhibition. Nature *590*, 486–491.

Davoli, T., Xu, A.W., Mengwasser, K.E., Sack, L.M., Yoon, J.C., Park, P.J., and Elledge, S.J. (2013). Cumulative haploinsufficiency and triplosensitivity drive aneuploidy patterns and shape the cancer genome. Cell *155*, 948–962.

DePristo, M.A., Banks, E., Poplin, R., Garimella, K.V., Maguire, J.R., Hartl, C., Philippakis, A.A., Del Angel, G., Rivas, M.A., Hanna, M., et al. (2011). A framework for variation discovery and genotyping using next-generation DNA sequencing data. Nat. Genet. *43*, 491–498.

Dobles, M., Liberal, V., Scott, M.L., Benezra, R., and Sorger, P.K. (2000). Chromosome missegregation and apoptosis in mice lacking the mitotic checkpoint protein Mad2. Cell *101*, 635–645.

Gemoll, T., Habermann, J.K., Becker, S., Szymczak, S., Upender, M.B., Bruch, H.P., Hellman, U., Ried, T., Auer, G., Jörnvall, H., and Roblick, U.J. (2013). Chromosomal aneuploidy affects the global proteome equilibrium of colorectal cancer cells. Anal. Cell. Pathol. (Amst.) *36*, 149–161.

Ghandi, M., Huang, F.W., Jané-Valbuena, J., Kryukov, G.V., Lo, C.C., Mcdonald, E.R., 3rd, Barretina, J., Gelfand, E.T., Bielski, C.M., Li, H., et al. (2019). Next-generation characterization of the Cancer Cell Line Encyclopedia. Nature *569*, 503–508.

Gómez-Miragaya, J., Díaz-Navarro, A., Tonda, R., Beltran, S., Palomero, L., Palafox, M., Dobrolecki, L.E., Huang, C., Vasaikar, S., Zhang, B., et al. (2019). Chromosome 12p amplification in triple-negative/*BRCA1*-mutated breast cancer associates with emergence of docetaxel resistance and carboplatin sensitivity. Cancer Res. *79*, 4258–4270.

Habermann, J.K., Paulsen, U., Roblick, U.J., Upender, M.B., Mcshane, L.M., Korn, E.L., Wangsa, D., Krüger, S., Duchrow, M., Bruch, H.-P., et al. (2007). Stage-specific alterations of the genome, transcriptome, and proteome during colorectal carcinogenesis. Genes Chromosomes Cancer *46*, 10–26.

Hewitt, L., Tighe, A., Santaguida, S., White, A.M., Jones, C.D., Musacchio, A., Green, S., and Taylor, S.S. (2010). Sustained Mps1 activity is required in mitosis to recruit O-Mad2 to the Mad1-C-Mad2 core complex. J. Cell Biol. *190*, 25–34.

Hoevenaar, W.H.M., Janssen, A., Quirindongo, A.I., Ma, H., Klaasen, S.J., Teixeira, A., Van Gerwen, B., Lansu, N., Morsink, F.H.M., Offerhaus, G.J.A., et al. (2020). Degree and site of chromosomal instability define its oncogenic potential. Nat. Commun. *11*, 1501.

Holohan, C., Van Schaeybroeck, S., Longley, D.B., and Johnston, P.G. (2013). Cancer drug resistance: an evolving paradigm. Nat. Rev. Cancer *13*, 714–726.

Jamal-Hanjani, M., Wilson, G.A., Mcgranahan, N., Birkbak, N.J., Watkins, T.B.K., Veeriah, S., Shafi, S., Johnson, D.H., Mitter, R., Rosenthal, R., et al. (2017). Tracking the evolution of non-small-cell lung cancer. N. Engl. J. Med. *376*, 2109–2121.

Janssen, A., Kops, G.J., and Medema, R.H. (2009). Elevating the frequency of chromosome mis-segregation as a strategy to kill tumor cells. Proc. Natl. Acad. Sci. USA *106*, 19108–19113.

Jun, G., Wing, M.K., Abecasis, G.R., and Kang, H.M. (2015). An efficient and scalable analysis framework for variant extraction and refinement from population-scale DNA sequence data. Genome Res. *25*, 918–925.

Kops, G.J., Foltz, D.R., and Cleveland, D.W. (2004). Lethality to human cancer cells through massive chromosome loss by inhibition of the mitotic checkpoint. Proc. Natl. Acad. Sci. USA *101*, 8699–8704.

Langmead, B., and Salzberg, S.L. (2012). Fast gapped-read alignment with Bowtie 2. Nat. Methods *9*, 357–359.

Levine, M.S., and Holland, A.J. (2018). The impact of mitotic errors on cell proliferation and tumorigenesis. Genes Dev. *32*, 620–638.

Li, H. (2011). A statistical framework for SNP calling, mutation discovery, association mapping and population genetical parameter estimation from sequencing data. Bioinformatics *27*, 2987–2993.

Lukow, D.A., Sausville, E.L., Chunduri, N.K., Leu, J., Smith, J.C., Kendall, J., Wang, Z., Storchova, Z., and Sheltzer, J.M. (2021). Chromosomal instability accelerates the evolution of resistance to anti-cancer therapies. bioRxiv. https://doi.org/10.1101/2020.09.25.314229.

Mason, J.M., Wei, X., Fletcher, G.C., Kiarash, R., Brokx, R., Hodgson, R., Beletskaya, I., Bray, M.R., and Mak, T.W. (2017). Functional characterization of CFI-402257, a potent and selective Mps1/TTK kinase inhibitor, for the treatment of cancer. Proc. Natl. Acad. Sci. USA *114*, 3127–3132.

McKenna, A., Hanna, M., Banks, E., Sivachenko, A., Cibulskis, K., Kernytsky, A., Garimella, K., Altshuler, D., Gabriel, S., Daly, M., and DePristo, M.A. (2010). The Genome Analysis Toolkit: a MapReduce framework for analyzing next-generation DNA sequencing data. Genome Res. *20*, 1297–1303.

Michel, L., Diaz-Rodriguez, E., Narayan, G., Hernando, E., Murty, V.V., and Benezra, R. (2004). Complete loss of the tumor suppressor MAD2 causes premature cyclin B degradation and mitotic failure in human somatic cells. Proc. Natl. Acad. Sci. USA *101*, 4459–4464.

Musacchio, A. (2015). The molecular biology of spindle assembly checkpoint signaling dynamics. Curr. Biol. *25*, R1002–R1018.

Nagashima, S., Soda, H., Oka, M., Kitazaki, T., Shiozawa, K., Nakamura, Y., Takemura, M., Yabuuchi, H., Fukuda, M., Tsukamoto, K., and Kohno, S. (2006). BCRP/ABCG2 levels account for the resistance to topoisomerase I inhibitors and reversal effects by gefitinib in non-small cell lung cancer. Cancer Chemother. Pharmacol. *58*, 594–600.

Ohashi, A., Ohori, M., Iwai, K., Nakayama, Y., Nambu, T., Morishita, D., Kawamoto, T., Miyamoto, M., Hirayama, T., Okaniwa, M., et al. (2015). Aneuploidy generates proteotoxic stress and DNA damage concurrently with p53-mediated post-mitotic apoptosis in SAC-impaired cells. Nat. Commun. *6*, 7668.

Orr, B., Talje, L., Liu, Z., Kwok, B.H., and Compton, D.A. (2016). Adaptive resistance to an inhibitor of chromosomal instability in human cancer cells. Cell Rep. *17*, 1755–1763.

Passerini, V., Ozeri-Galai, E., De Pagter, M.S., Donnelly, N., Schmalbrock, S., Kloosterman, W.P., Kerem, B., and Storchová, Z. (2016). The presence of extra chromosomes leads to genomic instability. Nat. Commun. *7*, 10754.

Pauer, L.R., Olivares, J., Cunningham, C., Williams, A., Grove, W., Kraker, A., Olson, S., and Nemunaitis, J. (2004). Phase I study of oral CI-994 in combination with carboplatin and paclitaxel in the treatment of patients with advanced solid tumors. Cancer Invest. *22*, 886–896.

Pavelka, N., Rancati, G., Zhu, J., Bradford, W.D., Saraf, A., Florens, L., Sanderson, B.W., Hattem, G.L., and Li, R. (2010). Aneuploidy confers quantitative proteome changes and phenotypic variation in budding yeast. Nature *468*, 321–325.

Pommier, Y., and Cushman, M. (2009). The indenoisoquinoline noncamptothecin topoisomerase I inhibitors: update and perspectives. Mol. Cancer Ther. *8*, 1008–1014.

Rancati, G., Pavelka, N., Fleharty, B., Noll, A., Trimble, R., Walton, K., Perera, A., Staehling-Hampton, K., Seidel, C.W., and Li, R. (2008). Aneuploidy

underlies rapid adaptive evolution of yeast cells deprived of a conserved cytokinesis motor. Cell *135*, 879–893.

Replogle, J.M., Zhou, W., Amaro, A.E., Mcfarland, J.M., Villalobos-Ortiz, M., Ryan, J., Letai, A., Yilmaz, O., Sheltzer, J., Lippard, S.J., et al. (2020). Aneuploidy increases resistance to chemotherapeutics by antagonizing cell division. Proc. Natl. Acad. Sci. USA *117*, 30566–30576.

Robey, R.W., Pluchino, K.M., Hall, M.D., Fojo, A.T., Bates, S.E., and Gottesman, M.M. (2018). Revisiting the role of ABC transporters in multidrug-resistant cancer. Nat. Rev. Cancer *18*, 452–464.

Roper, R.J., and Reeves, R.H. (2006). Understanding the basis for Down syndrome phenotypes. PLoS Genet *2*, e50.

Rutledge, S.D., Douglas, T.A., Nicholson, J.M., Vila-Casadesús, M., Kantzler, C.L., Wangsa, D., Barroso-Vilares, M., Kale, S.D., Logarinho, E., and Cimini, D. (2016). Selective advantage of trisomic human cells cultured in non-standard conditions. Sci. Rep. *6*, 22828.

Salgueiro, L., Buccitelli, C., Rowald, K., Somogyi, K., Kandala, S., Korbel, J.O., and Sotillo, R. (2020). Acquisition of chromosome instability is a mechanism to evade oncogene addiction. EMBO Mol. Med. *12*, e10941.

Santaguida, S., and Amon, A. (2015). Short- and long-term effects of chromosome mis-segregation and aneuploidy. Nat. Rev. Mol. Cell Biol. *16*, 473–485.

Santaguida, S., Richardson, A., Iyer, D.R., M'Saad, O., Zasadil, L., Knouse, K.A., Wong, Y.L., Rhind, N., Desai, A., and Amon, A. (2017). Chromosome mis-segregation generates cell-cycle-arrested cells with complex karyotypes that are eliminated by the immune system. Dev. Cell *41*, 638–651.e5.

Santaguida, S., Tighe, A., D'Alise, A.M., Taylor, S.S., and Musacchio, A. (2010). Dissecting the role of MPS1 in chromosome biorientation and the spindle checkpoint through the small molecule inhibitor reversine. J. Cell Biol. *190*, 73–87.

Santaguida, S., Vasile, E., White, E., and Amon, A. (2015). Aneuploidy-induced cellular stresses limit autophagic degradation. Genes Dev *29*, 2010–2021.

Santaguida, S., Vernieri, C., Villa, F., Ciliberto, A., and Musacchio, A. (2011). Evidence that Aurora B is implicated in spindle checkpoint signalling independently of error correction. EMBO J. *30*, 1508–1519.

Schonhoff, C.M., Park, S.W., Webster, C.R., and Anwer, M.S. (2016). p38 MAPK α and β isoforms differentially regulate plasma membrane localization of MRP2. Am. J. Physiol. Gastrointest. Liver Physiol. *310*, G999–G1005.

Selmecki, A., Forche, A., and Berman, J. (2006). Aneuploidy and isochromosome formation in drug-resistant Candida albicans. Science *313*, 367–370.

Selmecki, A.M., Dulmage, K., Cowen, L.E., Anderson, J.B., and Berman, J. (2009). Acquisition of aneuploidy provides increased fitness during the evolution of antifungal drug resistance. PLoS Genet. *5*, e1000705.

Sheltzer, J.M., Blank, H.M., Pfau, S.J., Tange, Y., George, B.M., Humpton, T.J., Brito, I.L., Hiraoka, Y., Niwa, O., and Amon, A. (2011). Aneuploidy drives genomic instability in yeast. Science *333*, 1026–1030.

Sheltzer, J.M., Ko, J.H., Replogle, J.M., Habibe Burgos, N.C., Chung, E.S., Meehl, C.M., Sayles, N.M., Passerini, V., Storchova, Z., and Amon, A. (2017). Single-chromosome gains commonly function as tumor suppressors. Cancer Cell *31*, 240–255.

Soto, M., Raaijmakers, J.A., Bakker, B., Spierings, D.C.J., Lansdorp, P.M., Foijer, F., and Medema, R.H. (2017). p53 prohibits propagation of chromosome segregation errors that produce structural aneuploidies. Cell Rep. *19*, 2423–2431.

Stingele, S., Stoehr, G., Peplowska, K., Cox, J., Mann, M., and Storchova, Z. (2012). Global analysis of genome, transcriptome and proteome reveals the response to aneuploidy in human cells. Mol. Syst. Biol. *8*, 608.

Tang, Y.C., Williams, B.R., Siegel, J.J., and Amon, A. (2011). Identification of aneuploidy-selective antiproliferation compounds. Cell *144*, 499–512.

Tarasov, A., Vilella, A.J., Cuppen, E., Nijman, I.J., and Prins, P. (2015). Sambamba: fast processing of NGS alignment formats. Bioinformatics *31*, 2032–2034.

Torres, E.M., Sokolsky, T., Tucker, C.M., Chan, L.Y., Boselli, M., Dunham, M.J., and Amon, A. (2007). Effects of aneuploidy on cellular physiology and cell division in haploid yeast. Science *317*, 916–924.

Trott, J., Tan, E.K., Ong, S., Titmarsh, D.M., Denil, S.L.I.J., Giam, M., Wong, C.K., Wang, J., Shboul, M., Eio, M., et al. (2017). Long-term culture of self-renewing pancreatic progenitors derived from human pluripotent stem cells. Stem Cell Rep. *8*, 1675–1688.

Van Den Bos, H., Bakker, B., Taudt, A., Guryev, V., Colomé-Tatché, M., Lansdorp, P.M., Foijer, F., and Spierings, D.C.J. (2019). Quantification of aneuploidy in mammalian systems. Methods Mol. Biol. 159–190.

Vasan, N., Baselga, J., and Hyman, D.M. (2019). A view on drug resistance in cancer. Nature *575*, 299–309.

Wang, S., Zhang, M., Liang, D., Sun, W., Zhang, C., Jiang, M., Liu, J., Li, J., Li, C., Yang, X., and Zhou, X. (2019). Molecular design and anticancer activities of small-molecule monopolar spindle 1 inhibitors: a medicinal chemistry perspective. Eur. J. Med. Chem. *175*, 247–268.

Weaver, B.A., and Cleveland, D.W. (2008). The aneuploidy paradox in cell growth and tumorigenesis. Cancer Cell *14*, 431–433.

Williams, B.R., Prabhu, V.R., Hunter, K.E., Glazier, C.M., Whittaker, C.A., Housman, D.E., and Amon, A. (2008). Aneuploidy affects proliferation and spontaneous immortalization in mammalian cells. Science *322*, 703–709.

Xie, J., Jin, B., Li, D.W., Shen, B., Cong, N., Zhang, T.Z., and Dong, P. (2014). ABCG2 regulated by MAPK pathways is associated with cancer progression in laryngeal squamous cell carcinoma. Am. J. Cancer Res. *4*, 698–709.

Zhang, C.Z., Spektor, A., Cornils, H., Francis, J.M., Jackson, E.K., Liu, S., Meyerson, M., and Pellman, D. (2015). Chromothripsis from DNA damage in micronuclei. Nature *522*, 179–184.

Zhu, J., Tsai, H.J., Gordon, M.R., and Li, R. (2018). Cellular stress associated with aneuploidy. Dev. Cell *44*, 420–431.

Zhu, L., and Chen, L. (2019). Progress in research on paclitaxel and tumor immunotherapy. Cell. Mol. Biol. Lett. *24*, 40.

Please cite this article in press as: Ippolito et al., Gene copy-number changes and chromosomal instability induced by aneuploidy confer resistance to chemotherapy, Developmental Cell (2021), https://doi.org/10.1016/j.devcel.2021.07.006



## STAR★METHODS

### KEY RESOURCES TABLE

| REAGENT or RESOURCE | SOURCE | IDENTIFIER |
|---|---|---|
| **Antibodies** | | |
| Anti-p38 MAPK alpha | Cell Signaling | Cat# 9218; RRID: AB_10694846 |
| Rabbit Anti-p38-delta MAP Kinase | Cell Signaling | Cat# 2308; RRID: AB_10694398 |
| Anti-Topoisomerase 1 | abcam | Cat# ab245431; RRID: AB_2891053 |
| ABCG2 (D5V2K) XP | Cell Signaling | Cat# 42078; RRID: AB_2799211 |
| Rabbit Anti-GAPDH | Cell Signaling | Cat# 2118; RRID: AB_561053 |
| Monoclonal Anti-Vinculin | Sigma-Aldrich | Cat# V9131; RRID: AB_477629 |
| Anti-α-Tubulin | Sigma-Aldrich | Cat# T9026; RRID: AB_477593 |
| Phospho-Histone H2A.X (Ser139) | Cell Signaling | Cat# 2577; RRID: AB_2118010 |
| Anti-Centromere Antibody | Antibodies Incorporated | Cat# 15-234-0001; RRID: AB_2687472 |
| Anti-phospho-Histone H3 (Ser10) | Sigma Aldrich | Cat# 06-570; RRID: AB_310177 |
| **Bacterial and virus strains** | | |
| pWZL Neo Myr Flag MAPK13 | Addgene | Cat# 20523 |
| **Chemicals, peptides, and recombinant proteins** | | |
| Reversine | Cayman Chemical | Cat# 10004412 |
| Topotecan | Tocris | Cat# 4562 |
| Trichostatin A | Tocris | Cat# 1406 |
| VER-155008 | Tocris | Cat# 3803 |
| Taxol | Tocris | Cat# 1097 |
| Indotecan | MedChemExpress | Cat# HY-18351 |
| Vamurafenim | Selleckchem | Cat# S1267 |
| Ciclopirox | Tocris | Cat# 6384 |
| Thio-TEPA | Sigma-Aldrich | Cat# 6069 |
| Vincristine sulfate | Sigma-Aldrich | Cat# V8388 |
| IOX 1 | Tocris | Cat# 4464 |
| Doxorubicin | Sigma-Aldrich | Cat# D1515 |
| Aphidicolin | Sigma-Aldrich | Cat# A0781 |
| Cisplatin (CCDP) | In house produced | N/A |
| 5-Fluorouracil (5-FU) | In house produced | N/A |
| Gemcitabine | In house produced | N/A |
| AZ3146 | Tocris | Cat# 3994 |
| SB203580 | Cell Signaling Technology | Cat# 5633S |
| BIRB 796 | Tocris | Cat# 5989 |
| Nocodazole | Sigma-Aldrich | Cat# M1404 |
| RO-3306 | Sigma-Aldrich | Cat# SML0569 |
| S-trityl-L-cysteine (STLC) | Sigma-Aldrich | Cat# T2509 |
| MG-132 | Tocris | Cat# 1748 |
| Torin1 | LC Laboratories | Cat# t-7887 |
| Ko143 | Sigma-Aldrich | Cat# K2144 |
| **Critical commercial assays** | | |
| Clarity Western ECL Substrate | Bio-rad | Cat# 1705061 |
| BCA Assay Kit | Thermo Fisher Scientific | Cat# 23225 |
| Criterion TGX Stain-Free Precast Gels | Bio-rad | Cat# 5678094 |
| RIPA Buffer (10X) | Cell Signaling Technology | Cat# 9806 |
| Crystal violet solution | Sigma Aldrich | Cat# V5265 |
| Fast SYBR Green Master mix | Thermo Fisher Scientific | Cat# 4385614 |

(*Continued on next page*)

Please cite this article in press as: Ippolito et al., Gene copy-number changes and chromosomal instability induced by aneuploidy confer resistance to chemotherapy, Developmental Cell (2021), https://doi.org/10.1016/j.devcel.2021.07.006





*Continued*

| REAGENT or RESOURCE | SOURCE | IDENTIFIER |
|---|---|---|
| Fibronectin | Sigma Aldrich | Cat# F1141 |
| OneScript Plus cDNA Synthesis Kit | abm | Cat# G236 |
| Pierce Cell Surface Biotinylation-isolation Kit | Thermo Fisher Scientific | Cat# A44390 |
| RNeasy Plus Mini Kit (250) | QIAGEN | Cat# 74136 |
| CellTiter-Glo | Promega | Cat# G7570 |
| Protease inhibitor cocktail | Sigma Aldrich | Cat# 539134 |
| Phosphatase inhibitor cocktail | Sigma Aldrich | Cat# 04906837001 |
| **Deposited data** | | |
| Whole-exome sequencing | https://www.ebi.ac.uk | Accession number: PRJEB44814 |
| Single-cell whole-genome sequencing | https://www.ebi.ac.uk | Accession numbers: PRJEB44693 PRJNA672256 |
| **Experimental models: Cell lines** | | |
| A549 | ATCC | Cat# CCL-185™ |
| NCI-H1975 | ATCC | Cat# CRL-5908™ |
| RKO | ATCC | Cat# CRL-2577™ |
| PANC-1 | ECACC | Cat# 87092802 |
| A375 | IZSBS | Cat# BS TCL 88 |
| RPE1 hTERT | ATCC | Cat# CRL-4000™ |
| DLD-1 | ATCC | Cat# CCL-221™ |
| HCT-116 | ATCC | Cat# CCL-247™ |
| NCI-H460 | ATCC | Cat# HTB-177™ |
| NCI-H838 | ATCC | Cat# CRL-5844™ |
| NCI-H1299 | ATCC | Cat# CRL-5803™ |
| HCC366 | DSMZ | Cat# ACC 492 |
| NCI-H358 | ATCC | Cat# CRL-5807™ |
| HPAF-II | ATCC | Cat# CRL-1997™ |
| SK-MEL-31 | ATCC | Cat# HTB-73™ |
| **Oligonucleotides** | | |
| *MAPK14* gene expression Fwd; 5-TGCACATGCCTACTTTGCTC-3 | This Paper | N/A |
| *MAPK14* gene expression Rev; 5-AGGTCAGGCTTTTCCACTCA -3 | This Paper | N/A |
| *MAPK13* gene expression Fwd; 5-GGGATGGAGTTCAGTGAGGA-3 | This Paper | N/A |
| *MAPK13* gene expression Rev; 5-GTCCTCATTCACAGCCAGGT-3 | This Paper | N/A |
| *MAPK13* gene expression Fwd; 5-GTCATTGGGCTCCTGGATGTCT-3 | This Paper | N/A |
| *MAPK13* gene expression Rev; 5-CACCAGGTACTGGATCTTCTCC-3 | This Paper | N/A |
| *ABCC1* gene expression Fwd; 5-TGTGTGGGCAACTGCATCG-3 | This Paper | N/A |
| *ABCC1* gene expression Rev; 5-GTTGGTTTCCATTTCAGATGACATCCG-3 | This Paper | N/A |
| *ABCG2* gene expression Fwd; 5-CCGCGACAGCTTCCAATGACCT-3 | This Paper | N/A |
| *ABCG2* gene expression Rev; 5-GCCGAAGAGCTGCTGAGAACTGTA-3 | This Paper | N/A |
| *GAPDH* gene expression Fwd; 5-CAACTACATGGTTTACATGTTC-3 | This Paper | N/A |
| *GAPDH* gene expression Rev; 5-GCCAGTGGACTCCACGAC-3 | This Paper | N/A |

(*Continued on next page*)

Please cite this article in press as: Ippolito et al., Gene copy-number changes and chromosomal instability induced by aneuploidy confer resistance to chemotherapy, Developmental Cell (2021), https://doi.org/10.1016/j.devcel.2021.07.006



*Continued*

| REAGENT or RESOURCE | SOURCE | IDENTIFIER |
|---|---|---|
| Software and algorithms | | |
| ImageJ | ImageJ | https://imagej.net/Fiji/Downloads |
| DepMap | DepMap | https://depmap.org/portal/ |
| Prism | GraphPad Prism | https://www.graphpad.com/scientific-software/prism/ |
| Image Lab | Image Lab Bio-rad | https://www.bio-rad.com/it-it/product/image-lab-software?ID=KRE6P5E8Z |

## RESOURCE AVAILABILITY

### Lead contact

Further information and requests for resources and reagents should be directed to and will be fulfilled by the Lead Contact, Dr. Stefano Santaguida (Stefano.Santaguida@IEO.it).

### Materials availability

Cell lines used in this study are available from the American Type Culture Collection (ATCC), or from the Lead Contact. Antibodies are available from the sources listed in the key resources table.

### Data and code availability

No software or custom code was generated for this study. The accession numbers for single-cell whole-genome sequencing data reported in this paper are PRJEB44693 and PRJNA672256. The accession number for whole-exome sequencing data reported in this paper is PRJEB44814.

## EXPERIMENTAL MODEL AND SUBJECT DETAILS

### Cell culture condition and reagents

All cell lines were tested free of mycoplasma contamination using Myco Alert (Lonza, Walkersville, MD, USA) according to the manufacturer's protocol. All cells were maintained in a humidified environment at 37 °C with 5% $CO_2$ and cultured in standard medium conditions.

### Drug treatments

Reversine was obtained from Cayman Chemical and used at a working concentration of 0,125 μM, 0,25 μM or 0,5 μM; Topotecan (working concentration 0,11 μM), Trichostatin A (working concentration 0,5 μM), VER 155008 (working concentration 5 μM), Taxol (working concentration 0,01 or 0,003 μM), Ciclopirox (working concentration 2 μM), IOX1 (working concentration 30 μM), AZ3146 (working concentration 1 or 2 μM), BIRB 796 (working concentration 1 μM) were purchased from Tocris; Vemurafenib (working concentration 1 μM) was purchased from Selleckchem; Doxorubicin (working concentration 0,2 μM), Aphidicolin (working concentration 0,4 μM), Ko143 (working concentration 1 μM), Thio TEPA (working solution 100 μM), Vincristine (working solution 0,1 μM) were purchased from Merck Sigma- Aldrich; SB203580 (working concentration 10 μM) was purchased from Cell Signaling Technology; Cisplatin (working concentration 1, 2 or 3,3 μM), 5-Fluoruracile (working concentration 3,5 or 9 μM) and Gemcitabine (working concentration 0,2 μM) were obtained from the hospital pharmacy at the European Institute of Oncology (Milan, Italy).

## METHOD DETAILS

### Cell proliferation Assay

NCI-H1975, A549, RKO, A375 and RPE1 hTERT cell lines at 50% of confluence, were treated with DMSO or reversine (0,125 μM, 0,25 μM or 0,5 μM) for 30hrs and then the drugs were washed out. After 12hrs, cells were plated in a 6well plate support and were counted after 3, 7, 11 and 15 days after plating using the Bürker counting chamber (Blaubrand, Germany). The experiment was performed in at least two technical replicates.

### RNA extraction, RT–PCR and qPCR

RNA was extracted from cells using RNeasy Plus Mini Kit (QIAGEN), according to manufacturer's protocol. 500 ng of RNA from each sample was reverse-transcribed using OneScript Plus cDNA Synthesis Kit (abm) according to the manufacturer's instructions. mRNA

expression was performed by real-time quantitative PCR reactions using Fast SYBR™ Green reaction mix (Thermo Fisher Scientific) and achieved on an Applied Biosystems 7500 Fast Real-time PCR system. The relative expression level was calculated with the $2^{[DDCt]}$ method and expressed as a ''fold change'': normalization of data was performed on house-keeping gene (*GAPDH*) expression and compared to the Parental cells as a control. Primers used for profiling the mRNA expression levels of genes are as follows: *MAPK14* Fwd: 5-TGCACATGCCTACTTTGCTC-3; Rev: 5-AGGTCAGGCTTTTCCACTCA-3; *MAPK13* Fwd: 5- GGGATGGAGTT CAGTGAGGA-3; Rev: 5-GTCCTCATTCACAGCCAGGT-3; *MAPK13* Fwd: 5- GTCATTGGGCTCCTGGATGTCT-3; Rev: 5-CACCA GGTACTGGATCTTCTCC-3; *ABCC1* Fwd: 5- TGTGTGGGCAACTGCATCG-3; Rev: 5-GTTGGTTTCCATTTCAGATGACATCCG-3; *ABCG2* Fwd: 5-CCGCGACAGCTTCCAATGACCT-3; Rev: 5-GCCGAAGAGCTGCTGAGAACTGTA-3; *GAPDH* Fwd: 5- CAACTA CATGGTTTACATGTTC-3; Rev: 5-GCCAGTGGACTCCACGAC-3.

### Protein detection by Western blots

For protein analyses, cells were lysed in RIPA 1x lysis buffer (RIPA buffer 10x; CellSignaling Technology) with the addition of protease inhibitor cocktail (Millipore), phosphatase inhibitor cocktail (Sigma Aldrich) and then sonicated. Protein lysates were centrifuged at maximum speed for 10 min and resolved on 15% SDS-PAGE gels. The following primary antibodies were used: anti-p38α MAPK (#9218; CellSignaling Technology, 1:1000), anti-p38δ MAPK (#2308; CellSignaling Technology; 1:1000), anti-Topoisomerase 1 (#ab2454311; abcam; 1:1000), anti-ABCG2 (D5V2K) XP Rabbit mAb (#42078; CellSignaling Technology; 1:1000), anti-GAPDH (#2118; CellSignaling Technology; 1:1000), anti-Vinculin (#V9131; Sigma-Aldrich; 1:1000), anti-Tubulin (#T9026; Sigma-Aldrich; 1:1000).

### Retrovirus production and infection of target cells

Sub confluent Phoenix-AMPHO cells were transfected using Calcium/Phosphate precipitation, with retroviral constructs pWZL Neo Myr Flag MAPK13 (addgene, #20523). After a double cycle of infection, NCI-H1975 target cells were selected with 1mg/ml neomycin.

### Cell imaging methods

For immunofluorescence imaging NCI-H1975, RKO, A375, A549 and RPE-1 cells were plated onto coverslips coated with 5 μg/ml Fibronectin (Sigma-Aldrich) at 50/60% confluence and synchronized with 7,5 μM RO-3306 (Sigma-Aldrich) for 24 hrs at 37°C. Cells were then washed three times with 1X PBS and treated with 125nM, 250nM and 500nM reversine (Cayman Chemical) or DMSO as vehicle control for 50 minutes at 37°C. Cells were treated with MG-132 (Tocris) for 90 minutes at 37°C. Cells were fixed with 4% paraformaldehyde (in PBS) for 15 minutes at room temperature and blocked in 5% BSA in PBS for 30 minutes and incubated with the following antibodies for 90 minutes at room temperature: anti-α-Tubulin (Sigma-Aldrich) 1:1500, anti- phospho-Histone H3 (Ser10) (Sigma Aldrich) 1:500, anti-centromeric antibody (Antibodies Incorporated) 1:100. Alexa 488-, Alexa Cy3- and Alexa 647-labeled secondary antibodies (Invitrogen) were used 1:400 for 45 minutes at room temperature. DAPI 1:5000 was used to stain DNA. Coverslips were mounted using Mowiol. Cells were imaged using Leica SP8 confocal microscope with a magnification objective of 63x. FIJI software was used for image processing.

### Video microscopy

Live cell imaging was performed using an inverted microscope (Nikon Eclipse Ti) with a 20x objective. The microscope was equipped with an incubation chamber maintained at 37°C in an atmosphere of 5% $CO_2$. For experiments described in Figures 1A, S1, S5B, and S5F, NCI-H1975, A549, RKO, A375 and RPE-1 hTERT expressing a GFP-tagged version of H2b were seeded on 12-well plates. Cells were then treated with DMSO or reversine (0,125 or 0,250 or 0,5 μM) and immediately filmed for 48 hrs. Images were acquired every 5 min. For each condition, 60 cells from two biological replicates were analyzed using FIJI software.

### Crystal violet assay

For colony assay, cells at 50% of confluence were treated with DMSO, reversine (0,25 or 0,5μM), Cis-Platin (1 μM) or Aphidicolin (0,4 μM) for 30hrs, Nocodazole (100ng/ml) or STLC (5μM) for 12hrs, Torin1 (1μM) for 15 days, and then the drugs were washed out. After 12hrs, 30.000 cells/well were plated in a 12well plate support and treated for 4 or 6 weeks with chemotherapeutic agents or vehicle control (DMSO), as indicated in figure legends. Growth medium (containing drugs or vehicle control) was changed every 4 days. At the end of the treatment, cells were washed twice with ice-cold PBS and fixed with ice-cold 4% PFA for 15 min. Afterward, 1% crystal violet solution (Sigma V5265) was added to the plates and incubated at room temperature for 15 min. Plates were then washed with distilled $H_2O$, until the unbound crystal violet was removed and plates were dried at room temperature. Crystal violet stained cells were quantified by incubating the plates with 10% Acetic Acid at room temperature for 30 min, on a shaker. Then, the absorbance of the solubilized crystal violet suspension derived from each single well was measured by spectrophotometer at a wavelength of 600 nm.

### EC50 assay

Cells were plated in 96-well plates (white flat bottom; Thermo Fisher Scientific), in triplicate in 50 μl of medium. The following day, cells were treated with drugs (Topotecan, Indotecan or Taxol) dissolved in 50 μl of medium. After 72h of treatment, 100 μl of CellTiter-Glo

reagent (Promega; Madison, WI) was added to each well; the plates were incubated at room temperature for 10 minutes and the luminescence signal was measured with a GloMax microplate reader (Promega; Madison, WI). Relative luminescence unit (RLU) was represented on the graphs.

### Plasma membrane purification

Cells were plated in 150mm plates, treated and cultured until 85-90% confluent. Plasma Membrane purification was performed using Pierce™ Cell Surface Protein Biotinylation and Isolation Kit following manufacturer's instructions for adherent cells; in the lysis step, protease inhibitor cocktail (Millipore) and phosphatase inhibitor cocktail (Roche) were added. Eluted proteins were quantified using Pierce™ BCA Protein Assays. Then, sample buffer was added to eluates and samples were analyzed by Western Blot.

### Multicolor fluorescence in situ hybridization (mFISH)

For mFISH analysis, cells were treated with colcemid (100 ng/ml, Roche) for 90 min and prepared as described in (Trott et al., 2017). Briefly, mitotic cells were collected by mitotic shake-off after a short trypsin treatment and centrifuged at 1000 rpm for 10 min. Cell pellets were resuspended in 75 mM KCl and incubated for 15 min in a 37°C waterbath. Carnoy fixative solution (methanol/acetic acid, 3:1) was prepared and 1:10 volume added on the cells, before centrifugation at 1000 rpm for 15 min. Cells were then fixed for 30 min at room temperature in the carnoy solution, centrifuged and washed once more with fixative. Minimum volume of fixative was left to resuspend the pellet and cells were dropped onto clean glass slides. mFISH staining was performed following manufacturer's instructions (MetaSystems). The Metafer imaging platform (MetaSystems) and the Isis software were used for automated acquisition of the chromosome spread and mFISH image analysis.

### Sample processing for single-cell sequencing

For single-cell sequencing, cells from a single well were pulled and pelleted. For single nuclei isolation, cell pellets were resuspended in lysis buffer (1M tris-HCl pH7.4, 5M NaCl, 1M CaCl2, 1M MgCl2, 7.5% BSA, 10% NP-40, ultra-pure water, 10 mg/ml Hoechst 33358, 2mg/ml propidium iodide) and kept on ice in the dark for 15 min to facilitate lysis. G1 single nuclei, as assessed by PI and Hoechst staining were sorted into 96 wells plates on a BD FacsJAZZ cell sorter (BD Biosciences) and stored in -80C until further analysis. For single cell libraries preparation, single nuclei were lysed and DNA was barcoded, followed by automated library preparation (Bravo Automated Liquid Handling Platform, Agilent Technologies) as described previously (Van Den Bos, 2019). Single cell libraries were pooled and analyzed on an Illumina Hiseq2500 sequencer.

### Data analysis single-cell sequencing

Sequencing was performed using a NextSeq 500 machine (Illumina; up to 77 cycles; single end). The generated data were subsequently demultiplexed using sample-specific barcodes and changed into fastq files using bcl2fastq (Illumina; version 1.8.4). Reads were afterwards aligned to the human reference genome (GRCh38/hg38) using Bowtie2 (version 2.2.4; (Langmead and Salzberg, 2012)). Duplicate reads were marked with BamUtil (version 1.0.3; (Jun et al., 2015)).

The aligned read data (bam files) were analyzed with a copy number calling algorithm called AneuFinder (https://github.com/ataudt/aneufinder; (Bakker et al., 2016)). Following GC correction and blacklisting of artefact-prone regions (extreme low or high coverage in control samples), libraries were analyzed using the dnacopy and edivisive copy number calling algorithms with variable width bins (average binsize = 1 Mb).

Results were afterwards curated by requiring a minimum concordance of 95% between the results of the two algorithms. Libraries with on average less than 10 reads per bin (~ 30,000 reads for a diploid genome) were discarded.

The aneuploidy score of each bin was calculated as the absolute difference between the observed copy number and the expected copy number when euploid. The score for each library was calculated as the weighted average of all the bins (size of the bin as weight) and the sample scores were calculated as the average of the scores of all libraries.

Heterogeneity scores were calculated with two different methods. The heterogeneity scores of A375 and A549 were calculated with a more recent introduced method. Using this method, the heterogeneity score of each bin was calculated as the proportion of pairwise comparisons (cell 1 vs. cell 2, cell 1 vs cell 3, etc.) that showed a difference in copy number (e.g. cell 1: 2-somy and cell 2: 3-somy). The heterogeneity score of each sample was calculated as the weighted average of all the bin scores (size of the bin as weight). The heterogeneity scores of the remaining samples were calculated with the original method (Bakker et al., 2016).

The structural score of each library was calculated as the number of detected breakpoints (number of copy number transitions) divide by the total genome length in Mb (average number of breakpoints per Mb). The structural score of each sample was calculated as the average structural score of all libraries.

scWGS have been deposited to SRA with BioProject accession number PRJEB44693. SS35 and SS48 have been deposited to SRA with BioProject PRJNA672256 (accession number SRR14381438 for SS35 and SRR12904712 for SS48). SS48 has been reported in (Cohen-Sharir et al., 2021).

### Detection of SNPs and small indels

The first steps of the analysis (alignment and calling variants) were performed by the Genomics Coordination Center at the University Medical Center of Groningen, The Netherlands. The complete pipeline is described in detail at the following webpage:https://molgenis.gitbooks.io/ngs_dna/content/ngs-protocols.html

Please cite this article in press as: Ippolito et al., Gene copy-number changes and chromosomal instability induced by aneuploidy confer resistance to chemotherapy, Developmental Cell (2021), https://doi.org/10.1016/j.devcel.2021.07.006





In short: Sequencing reads were aligned to the human reference genome (GRCh37) with the BWA mem program (version 0.7.15-foss-2015b) using default settings. Aligned reads were subsequently sorted with the SortSam tool from Picard (version 2.9.0-Java-1.8.0_74; Broad Institute). The BaseRecalibrator tool from GATK was afterwards used to recalibrate the quality scores of the bases (default settings; version 3.7-Java-1.8.0_74; (DePristo et al., 2011; McKenna et al., 2010)) and duplicate reads were marked with the markdup tool from sambamba (version v0.6.6-foss-2015b; (Tarasov et al., 2015)). Variants were called with the HaplotypeCaller tool from GATK and genotyped using GenotypeGVCFs (default settings) both from GATK. SNPs and indels were finally filtered using several quality parameters of GATK. Filtering expression SNPs: "QD < 2.0", "FS > 60.0", "MQ < 25.0", "MQRankSum < -12.5", "ReadPosRankSum < -8.0"; Indels: "QD < 2.0", "FS > 200.0", "ReadPosRankSum < -20.0".

The above described pipeline is used for diagnostics and was not updated for the latest genome build. The genomic coordinates were therefore mapped to GRCh38 using the Assembly Converter tool of Ensembl (Web: https://www.ensembl.org/Homo_sapiens/Tools/AssemblyConverter) and also with the Lift Genome Annotations tool from UCSC (Web: https://genome.ucsc.edu/cgi-bin/hgLiftOver). Non-matching coordinates came from variable genomic patches and were excluded for further analysis (1,145 variants; 2.1 %).

Variant files were subsequently sorted and indexed using the sort and index tools from bcftools (version 1.9; using htslib version 1.9; (Li, 2011)). IDs of known SNPs, dbSNPs, were added to the variants with the annotate tool from bcftools. The dbSNPs from the GATK Resource Bundle were used for this purpose (Web: https://gatk.broadinstitute.org/hc/en-us/articles/360035890811-Resource-bundle; file: Homo_sapiens_assembly38.dbsnp138.vcf). Gene and variant effect annotations (effect on gene / protein functioning; amino acid changes etc.) were added to the variants with the use of SnpEff (ann: GRCh38.99; version: 5.0e; (Cingolani et al., 2012)). A few variants were excluded because of changes in the reference sequence (833 variants; 1.5 %).

Variants were, in addition to the above described variant filtration by GATK, also filtered based on read depth and genotype quality (>= 20). Variants were first filtered based on a minimum combined read depth of 30 and a maximum combined read depth of 2,000. For subsequent paired analysis (parent vs. TRP-DMSO; parent vs. TRP-Mps1i) variants were required to have a minimum read depth of 10 and a maximum read depth of 600 (individual samples).

The possible impact of clonal mutations on chemoresistance was quantified by calculating the proportion of reads that support a variant that is detected for TRP-DMSO or TRP-Mps1i but not for the parent. This proportion or ''alternative ratio'' (AR) was introduced in order to prioritize (rank) variants. Three different categories were considered (AR >= 0.1, 0.5 and 0.9).

$$\mathrm{AR}[\mathrm{TRP-DMSO\ or\ TRP-Mps1i}] = \frac{\text{Number of reads supporting the variant(allele depth; AD)}}{\text{Total read depth at the position (DP)}}$$

(AD parent = 0 for these variants)Whole-exome sequencing data have been deposited to SRA with BioProject accession number PRJEB44814.

### Co-expression analysis of *ABCG2* with genes residing on chromosome 6

mRNA expression levels were obtained from the CCLE gene expression data set (19q4 DepMap release; CCLE_mutations.csv) (Ghandi et al., 2019). A gene expression linear association analysis was performed in the DepMap portal (https://depmap.org/portal/), using ABCG2 expression as the dependent variable and the dataset as the independent variable. The analysis regresses a dependent variable on an independent variable and reports a moderated regression coefficient along with its p-value and q-value.

## QUANTIFICATION AND STATISTICAL ANALYSIS

Statistical analysis was performed using GraphPad Prism software. Details of the statistical tests were reported in figure legends. Error bars represent SD or SEM. All experiments were performed in two or more replicates.